Journal of Structural Biology: X 6 (2022) 100066

Contents lists available at ScienceDirect

Journal of Structural Biology: X

journal homepage: www.sciencedirect.com/journal/journal-of-structural-biology-x

Review Article

Not making the cut: Techniques to prevent RNA cleavage in structural studies of RNase–RNA complexes

Seth P. Jones [a], Christian Goossen [a,b], Sean D. Lewis [a,c], Annie M. Delaney [a], Michael L. Gleghorn [a,*]

[a] School of Chemistry and Materials Science, Rochester Institute of Technology, 85 Lomb Memorial Drive, Rochester, NY 14623-5603, United States
[b] Pittsburgh Heart, Lung, Blood and Vascular Medicine Institute, University of Pittsburgh, Lothrop St, Pittsburgh, PA 15261, United States
[c] Mayo Clinic, 200 1st St SW, Rochester, MN 5590, United States

ARTICLE INFO

Keywords:
RNase–RNA complex
Pre-cleavage
Scissile-phosphate
Structure determination
Enzymatic inhibition
Nucleic acid recognition

ABSTRACT

RNases are varied in the RNA structures and sequences they target for cleavage and are an important type of enzyme in cells. Despite the numerous examples of RNases known, and of those with determined three-dimensional structures, relatively few examples exist with the RNase bound to intact cognate RNA substrate prior to cleavage. To better understand RNase structure and sequence specificity for RNA targets, *in vitro* methods used to assemble these enzyme complexes trapped in a pre-cleaved state have been developed for a number of different RNases. We have surveyed the Protein Data Bank for such structures and in this review detail methodologies that have successfully been used and relate them to the corresponding structures. We also offer ideas and suggestions for future method development. Many strategies within this review can be used in combination with X-ray crystallography, as well as cryo-EM, and other structure-solving techniques. Our hope is that this review will be used as a guide to resolve future yet-to-be-determined RNase–substrate complex structures.

Introduction

In this review of methods to assemble ribonuclease (RNase)–RNA complexes trapped in a pre-cleavage state, the catalytic mechanisms of these discussed RNases, in general, fall within two major categories (Table 1). Regardless of category, a scissile phosphate is attacked by an activated oxygen that breaks a nucleotide linking O-P bond. The first category of metal dependent RNases can be divided further into those that derive the attacking oxygen from water (i.e. hydrolytic; Fig. 1A), and those that use anionic inorganic phosphate to provide the attacking oxygen, subsequently substituting for the bridging 2′-O of the scissile phosphate (i.e. phosphorolytic; Fig. 1B). When the nucleophile derives from water, the resulting product is a 3′–OH and 5′-PO_4 as cut-site terminal end products on the resulting 5′ and 3′ RNA pieces, respectively (Fig. 1A) (Frazão et al., 2006; Samara and Yang, 2018). When the nucleophile derives from phosphate, products contain a 3′–OH on the 5′ piece and a 5′-diphosphate on the 3′ piece that is a nucleoside diphosphate (NDP) since known phosphorylases are 3′ exoribonucleases (Fig. 1B). In the second major category, that of metal independent RNases, the attacking oxygen derives from the 2′–OH group of the nucleotide that is 5′ to the cut-site. Unlike metal dependent RNase mechanisms, 2′-O nucleophilic attack results in a 5′–OH on the 3′ piece with a 2′,3′-cyclic-PO_4 intermediate formed on the 5′ piece that is then converted by hydrolysis in a second step to a 3′-PO_4 and 2′–OH (Fig. 1C) (Cuchillo et al., 2011; Mignon et al., 2002).

For metal dependent hydrolytic mechanisms, bound metals are used to: i) indirectly facilitate deprotonation of H_2O to activate the oxygen for nucleophilic attack, and ii) stabilize the transition state (Fig. 1A) (Howard et al., 2012; Li de la Sierra-Gallay et al., 2005; Schultz and Champoux, 2008; Steitz and Steitz, 1993; Sun et al., 2005; Warnecke et al., 2000; Zhao et al., 2015). For phosphorolytic RNases, an oxygen of inorganic phosphate is the scissile phosphate-attacking nucleophile (Fig. 1B; Navarro et al., 2008). While metals are thought to be important for such a mechanism (Unciuleac et al., 2021), the details of this are still limited and require further detailed study (Yang, 2011). Interestingly, phosphorolytic RNases can perform non-templated RNA polymerization in the reverse reaction using nucleotide diphosphates as substrates (Carzaniga et al., 2017). For metal independent acid-base mechanisms it is enzyme active site residues that activate the 2′–OH oxygen by having appropriate pKa values for proton removal (Fig. 1C) (Carte et al., 2010;

* Corresponding author.
E-mail address: mlgsch@rit.edu (M.L. Gleghorn).

https://doi.org/10.1016/j.yjsbx.2022.100066
Received 2 March 2022; Accepted 4 March 2022
Available online 11 March 2022

Table 1
RNase–RNA complex assembly techniques identified in our survey as they relate to each cleavage mechanism category.

Trapping method	RNase cleavage mechanism category		
	Metal dependent		Metal independent
	Hydrolytic (H_2O)	Phosphorolytic (PO_4)	Acid-Base (2′-OH)
Modification of RNA substrate			
Phosphate modification	YES	NO	NO
Sugar modification	YES	NO	NO
RNA base(s) sequence change	YES	NO	NO
Protein mutagenesis	YES	NO	YES
Crystallization solution manipulation	YES	YES	NO
RNase inhibitors	YES	NO	YES
Temperature snapshots	YES	NO	NO

Han et al., 2014; Ishii et al., 2003; Loverix et al., 2000; Luhtala and Parker, 2010; Schultz et al., 1998; Zorzini et al., 2016).

Despite there being only two major categories of RNase mechanisms (three categories if counting both types of metal dependent mechanisms; Fig. 1A–C) for cleavage of RNA polymers, there is a tremendous breadth of RNA substrate sequences, shapes, and cleavage site specificities. To determine the appearance, placement, and attributes of bound RNA substrate, structural studies of relevant RNase–RNA complexes captured prior to RNA cleavage are essential. In our examples below, it is the differences in RNase structures that permit a diverse repertoire of respective cognate substrate specificities. As part of acting on a broad range of RNA substrates, RNases are consequently involved in many important biological pathways (Bechhofer and Deutscher, 2019). The diversity and dynamic roles of RNases in cells have made them an important topic in medicine (Becknell et al., 2015; Henneke et al., 2009; Lewis, 2007; Wang et al., 2017). RNase prominence in biotechnology has exploded recently due to discoveries involving the CRISPR-Cas systems (Burmistrz et al., 2020). Cas9 and 13 have been implemented in RNA tracking and virus detection including for the 2019-novel corona virus (Aman et al., 2018; Freije et al., 2019; Hou et al., 2020; Kellner et al., 2019; Nelles et al., 2016). RNases are also used in DNA extraction, RNA binding protein purification, next generation sequencing, footprinting, mRNP position elucidation on an mRNA, and can be detected by RNase responsive DNA nanoswitches among other applications (Chandrasekaran et al., 2020; El-Ashram et al., 2016; Healey et al., 2014; Kang et al., 2019; Nilsen, 2014; Singh et al., 2017). All above examples depend on an abundant knowledge of RNase–RNA binding specificity that is often understood through structural biology, and historically, as evidenced by the many examples in this review, more so by X-ray crystal structure determinations.

Even with modern techniques, forming an intact protein–substrate

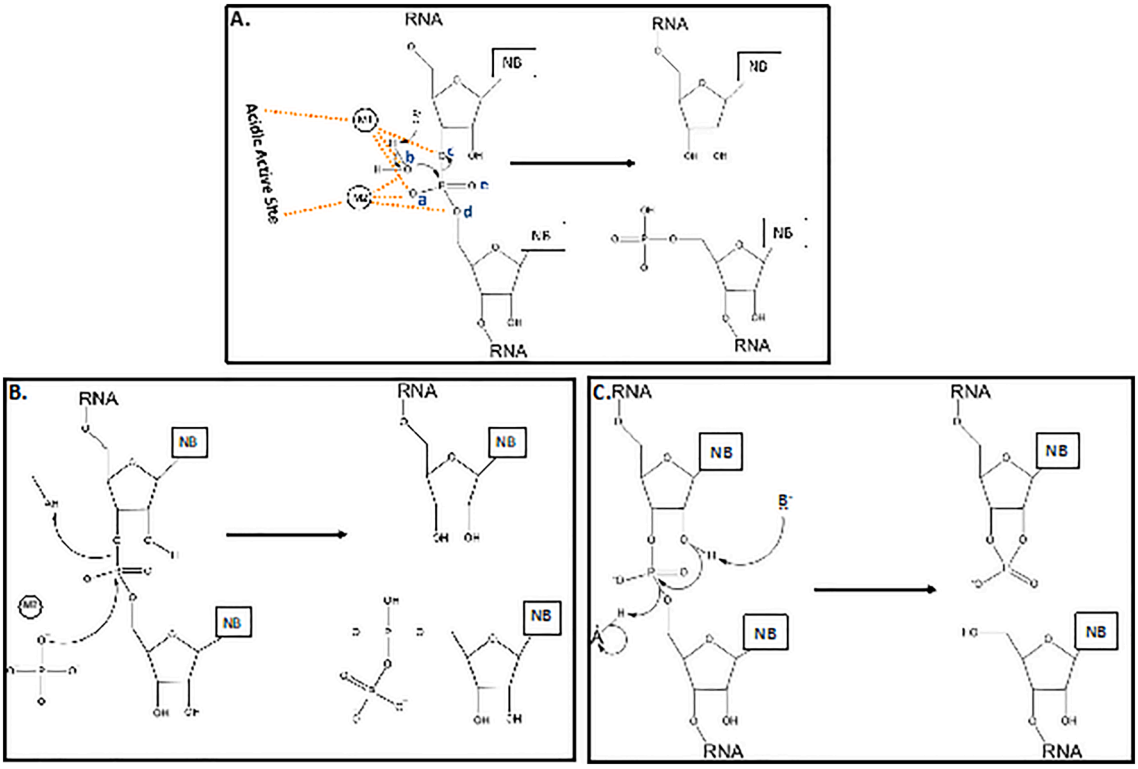

Fig. 1. Generalization of RNase mechanistic processes to activate oxygen for scissile phosphate attack. A.) A generalized mechanism for two-metal RNA hydrolysis. Nucleobases (A, C, G, or U) are indicated as "NB" to make distinct from the active site base "B" involved in catalysis. Depending on the enzyme, metals M1 and M2 can interact with several combinations of oxygens labeled "a", "b", "c", "d", and "e" in which interaction with "a", "c", "d", and "e" are for stabilization, and interaction with "b" is for activation of the phosphate-attacking nucleophile. Nucleophile activation is achieved by metal ions that draw electrons from the oxygen of H_2O ("b"), thus promoting deprotonation by an active site base. Then, the oxygen from the resulting OH^- attacks the scissile phosphate. The result of this mechanism is a 3′-O–P bond break leaving a 5′-PO_4 (one of these oxygens derive from what was originally H_2O) and a 3′-O that is protonated to become a 3′–OH. B.) A mechanism for RNases that utilize phosphate as the scissile-phosphate-attacking nucleophile; the attacking inorganic PO_4 becomes part of the 5′ di-phosphate terminal end produced in the generation of the 3′ product piece. A proton is contributed by an active site residue to establish the 3′–OH terminal end of the 5′ piece. This mechanism displayed derived from that put forth by Navarr et al. (Navarro et al., 2008), however we have added "M?" to indicate the potential roles of metals that need further structural elucidation to better understand. C.) A general mechanism for acid-base catalysis utilizing the 2′-O of the RNA nucleotide that is 5′ to the cut-site. The protonated residue stabilizes the leaving group and the basic residue deprotonates the 2′-O, activating it as the nucleophile, which attacks the scissile phosphate and forms the 2′,3′ cyclic pentacovalent intermediate.

complex poses a great challenge when the process is inherently and naturally transient and leads to a cleaved product. To reduce the difficulty for future researchers in determining the proper tactic to choose to capture a specific RNase–RNA complex for structure determinations, we describe here a number of strategies that have been successfully implemented. As a first step, especially to structurally elucidate RNase binding specificity recognition mechanisms of RNA, one needs to first understand the different possible RNase catalytic and binding mechanisms in general; this will guide the choice(s) of the proper engineered modification(s) to sustain RNA substrate binding to the RNase while simultaneously inhibiting RNA cleavage. We have scanned the Protein Data Bank for determined RNase–RNA pre-cleavage complexes and have categorized into different groups the successful strategies that were used. The different strategy groups that we discuss in this review include: modification of RNA substrate, protein mutagenesis, crystallization solution manipulation, RNase inhibitors, and temperature snapshots (Table 1). Importantly, some structures have been determined by using combined approaches, using more than one strategy at the same time. We also provide ideas and considerations that we think hold promise for the future. These methods will be important to ongoing efforts to detail the specificity of RNA recognition of a variety of RNases that are known and those likely yet-to-be revealed. Additionally, by trapping a pre-cleavage state, we can better understand the precise enzymatic details of RNases towards developing molecular tools to inhibit them if they are part of a virus and/or disease state, for example (s). This guide will not only be useful for RNase structural biologists but hopefully will inspire improved future method development as well.

Modification of RNA substrate

Chemical modifications of RNA substrates change the atomic-level details and properties of the substrate-interface of the substrate–enzyme complex (Table 2). Depending on the changes made, RNA can be manipulated to have lower or even totally inhibited cleavage reaction rates.

Phosphate modification

As the first example of a technique to inhibit RNase cleavage of RNA (and/or DNA cleavage by a nuclease able to cut DNA and RNA), phosphate backbone oxygens can be substituted with sulfur to inhibit RNases with metal-dependent mechanisms (i.e. phosphor(di)thioate) (Song et al., 2017; Wilson et al., 1995). Bridging nucleotide phosphates are not chiral, however, this phosphorothioate modification chemistry can produce chiral Rp (Fig. 2A, left) and Sp (Fig. 2A, right) stereoisomers (based off of the R, S nomenclature system). These two stereoisomers differ in the non-bridging phosphate oxygen that is substituted with sulfur; each isomer differently affects nuclease substrate preference and cleavage activity (Freudenthal et al., 2015; Warnecke et al., 1996; Wilson et al., 1995). An RNase III–RNA inhibited complex crystal structure (Table 2; PDB: 5T16) was determined by phosphorothioate modification that was associated with interrupted active site metal binding (Song et al., 2017). For a similar modification in an RNase P–RNA complex, Sp and Rp isomers also exhibited activity reduction but the RNase binding affinity of the Sp isomer was less, relative to Rp (Warnecke et al., 1996). Apurinic-apyrimidinic (AP) endonuclease 1

Table 2
RNase–RNA structures solved using a modified RNA substrate.

RNase	PDB ID	Substrate used for crystallization	Modification	Author
Homo sapiens AP endonuclease (APE1)	5DG0	21 mer dsDNA with an abasic site opposite a G-base at position 11, and a 2′-O-CH_3 modified nucleotide 3′ to the cut-site	Phosphorothioate modification of scissile phosphate as part of the abasic sugar-phosphate	(Freudenthal et al., 2015)
Saccharomyces cerevisiae S288C RNase III	5T16	34 mer dsRNA pseudo-duplex joined by a pair of 2 nucleotide 5′ overhangs	Phosphorothioate modification of a scissile phosphate	(Song et al., 2017)
Influenza A virus PA subunit N-terminus (PA_N) endonuclease	7KL3	6 mer ssRNA	Sulfur replacement of a phosphorus generating a sulfate (rather than phosphate) bridging the 2nd and 3rd nucleotides	(Kumar et al., 2021)
Escherichia coli (strain K12) RNase E	2C0B 2BX2	13 mer ssRNA 15 mer ssRNA	2′-O-CH_3 modification on the entire strand; authors did not model CH_3	(Callaghan et al., 2005)
Thermus thermophilus HB27 RNase J	3T3N	6 mer ssRNA	2′-O-CH_3 modification on the entire strand	(Dorléans et al., 2011)
Bacillus subtilis (subspecies subtilis strain 168) RNase Z	4GCW	pre-tRNA(Thr)	2′-O-CH_3 modification to the discriminator nucleotide and the trailer sequence (both sides of the cut site)	(Pellegrini et al., 2012)
Bacillus halodurans RNase H	5SWM	12 mer FRNA/DNA hybrid	2′-F modification on the entire RNA strand	(Pallan et al., 2016)
Thermos thermophilus Cas 6 (TTHA0078)	4C8Y	16 mer R1 repeat RNA containing a stem-loop structure	RNA → DNA at the G-nucleotide 5′ to the cut-site	(Niewoehner et al., 2014)
Escherichia coli RNase I	2Z70	7 mer ssDNA	RNA → DNA modification of the entire strand	(Rodriguez et al., 2008)
Bacillus subtilis (strain 168) MazF	4MDX	9 mer ssRNA	RNA → DNA at the U-nucleotide 5′ to the cut-site	(Simanshu et al., 2013)
Lithobates catesbeiana RNase A	1M07	4 mer ssDNA	RNA → DNA modification of the entire strand	(Leu et al., 2003)
Aspergillus oryzae RNase T1	1B2M	Guanylyl(3′-6′)-6′-deoxyhomouridine	A 5′-O → CH_2 modification	(Arni et al., 1999)
Human immunodeficiency virus 1 RNase H	6BSJ	An RNA/DNA hybrid duplex formed from a 25 mer RNA and a 23 mer DNA	An RNA/DNA hybrid that was optimized for DNA and RNA overhang length as well as to contain a −5/-4 AU sequence and a −2 G relative to the cut-site	(Lan et al., 2018; Tian et al., 2018)
Escherichia coli RNase T	3NGZ	5′-GC-3′ (note that the enzyme in this structure has an E92G mutation, yet retains catalytic activity)	A 3′ terminal C causes an inactive conformation	(Hsiao et al., 2011)
	3NH0	5′-d(TTACAAC)-3′ ssDNA from ($P2_12_12$ space group)		
	3NH2	5′-d(TTACAAC)-3′; forms a duplex with a two base overhang when bound to RNase T (P1 space group)		
Mycoplasma genitalium RNase R	7DID	4 mer ssRNA	2′-O-CH_3 modification at position 3	(Abula et al., 2021)

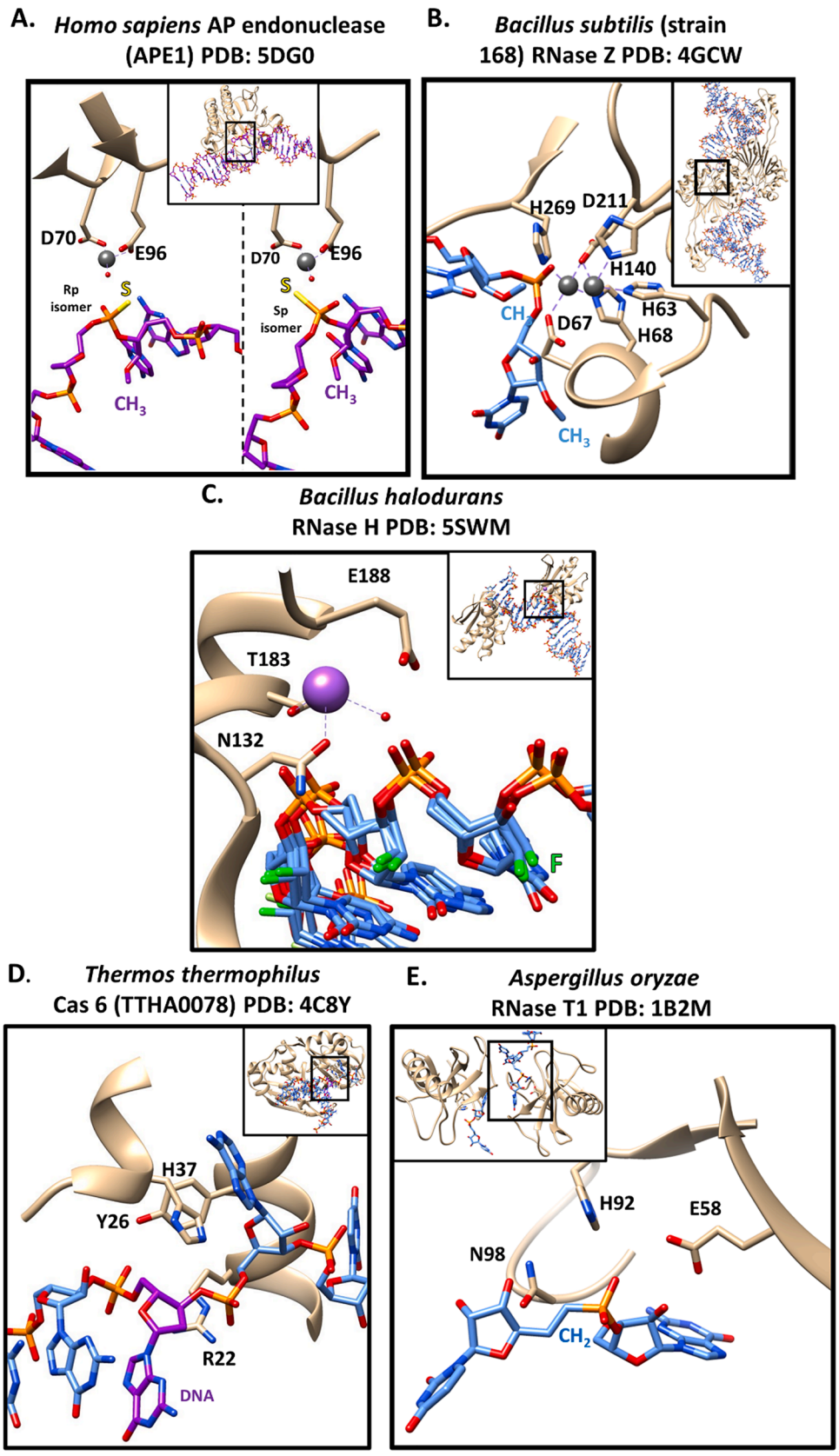

Fig. 2. Representative structures that utilize a chemical modification in RNA to capture an RNase–RNA pre-cleavage complex. The following standard convention will be used throughout figures in this review. Colors for macromolecules are as follows: RNase (ribbons and carbons), tan; RNA carbons, cornflower blue; and DNA carbons, purple. Colors for non-carbon atoms: O, red; N, blue; P, orange; S, yellow; F, green; divalent metals (Mg^{2+}, Mn^{2+}, and Zn^{2+}), dim grey; Na^{+}, purple; Ca^{2+}, hot pink. A.) 1.80 Å resolution X-ray crystal structure of *Homo sapiens* AP endonuclease I in complex with Rp isomer (left) and Sp isomer (right) phosphorothioate modified DNA and one Mn^{2+}. B.) 3.00 Å resolution X-ray crystal structure of *Bacillus subtilis* RNase Z in complex with pre-$tRNA^{Thr}$ having 2′-O-CH_3 modifications on each side of the cut site and two Zn^{2+} ions. C.) 1.5 Å resolution X-ray crystal structure of *Alkalihalobacillus halodurans* RNase H D132N in complex with a FRNA/DNA hybrid and one Na^{+}. D.) 1.80 Å resolution X-ray crystal structure of *Thermus thermophilus* HB8 in complex with an RNA → DNA modified RNA. E.) 2.00 Å resolution X-ray crystal structure of *Aspergillus oryzae* RNase T1 complexed with 5′-O → CH_2 modified RNA. In this, and in subsequent figures depicting X-ray crystal structures: images were generated using UCSF Chimera (Pettersen et al., 2004), insets represent a full view of the X-ray crystal structure, and are within a larger image of a view of the active site with important amino acid residues indicated. (For interpretation of the references to colour in this figure legend, the reader is referred to the web version of this article.)

(APE1) is an enzyme that has shown both RNase and DNase activity (Kim et al., 2010); the structure of *Homo sapiens* APE1 bound to 21 mer dsDNA has been determined by engineering an abasic site opposite a G-base (at position 11), and a 2′-O-CH_3 modified nucleotide (ligand id OMC) 3′ to a cut-site that had a phosphorothioate modification (Table 2; Fig. 2A; (Freudenthal et al., 2015). Both the Sp and Rp isomers were modeled in the crystal structure with near equal occupancy. Only the Sp isomer was oriented correctly for the hydrolysis reaction to occur, although it did not, due to lack of RNase activity in the presence of phosphorothioate; the Rp isomer (also not cleaved) was displaced from the active site by 2.1 Å. While the next example is not of an RNA polymer pre-cleavage state, phosphorothioate modification can also be applied to 2′,3′ cyclic intermediates to slow cleavage in the second half of an RNase reaction involving an acid-base mechanism; this is important to structurally characterize the full two-step mechanism. In this example, a crystal structure of RNase T1 in complex with unhydrolyzed guanosine-2′,3′-cyclophosphorothioate (PDB: 1GSP) was solved to study the intermediate step of the cleavage reaction (Zegers et al., 1998). The phosphorothioate modification slowed the reaction enough to allow for multiple crystal structures to be solved over a several-month period revealing the mechanism of this hydrolysis reaction (Zegers et al., 1998).

A different type of sulfur modification, albeit in the context of a point mutation designed to inhibit RNase activity, was used to determine the X-ray crystal structure of the N-terminal domain of the PA endonuclease (PA_N) subunit, one of three subunits of an influenza A RNA dependent RNA polymerase, bound to intact ssRNA (Table 2; (Kumar et al., 2021). Here, a sulfur substitution of phosphorous was introduced at the scissile phosphate position between a GC sequence. No metals were modeled in this structure and the expected register of this RNA within the active site for GC recognition and cleavage was not observed; the authors therefore structurally characterized this RNase–RNA interaction using other structures they determined and with computational modeling.

Sugar modification

In acid-base mechanisms that use activation of the ribose 2′–OH group that is 5′ to the cut site, this moiety can itself be altered to inhibit RNA cleavage by an RNase. As an example, a methyl group covalently attached to the 2′-O inherently hinders the nucleophilicity of the oxygen and also sterically inhibits the cleavage reaction. Since self-cleavage, and cleavage from contaminating 2′-O activation-dependent RNases can cause unwanted RNA degradation in any RNA-related experiment, 2′-O-methylation preserves the integrity of RNA even when the RNase being studied does not use a 2′-O related acid-base mechanism. In fact, in all of the RNase–RNA complex structures examples we surveyed, when 2′-O-methylated RNA was used to determine the structure (Table 2), the RNases were metal-dependent and likely did not require this modification to inhibit cleavage. In terms of binding, 2′-O-CH_3 modification is not always without cost, as binding kinetics studies of *Escherichia coli* RNase HI have shown that this modification causes substrate to bind weaker than natural substrate (Haruki et al., 1997). However, in the context of the high concentrations of macromolecules often used in crystallization, as long as the substrate remains bound in the correct orientation, the strength of the interaction can be overcome and mimic RNA binding within RNase active sites. Since metal-dependent mechanisms typically do not directly involve the 2′–OH, 2′-O-methylated RNAs are used in unison with inhibitory RNase mutations as in the structure of *Thermos thermophilus* RNase J, an enzyme that is involved in 5′ RNA maturation, where the H77A mutated protein was determined bound to 2′-O-methylated ssRNA, which mimics (i.e. represents) mRNA (Table 2; PDB: 3T3N; (Dorléans et al., 2011). Another example is the X-ray crystal structure of *Escherichia coli* RNase E in complex with fully 2′-O-CH_3 modified single-stranded RNA (ssRNA) substrate (Table 2; PDBs: 2C0B, 2BX2; (Callaghan et al., 2005). In the structure of *Bacillus subtilis* RNase Z bound to precursor tRNA (Table 2; Fig. 2B), authors describe the use of 2′-O-CH_3 modifications of a discriminator nucleotide (U73) and trailer sequence (U74-A75-A76) to inhibit cleavage between U73 and U74 (Pellegrini et al., 2012); these nucleotides are positioned at the 3′ terminal end of the tRNA and are likely more susceptible to contamination-derived degradation than more internal areas of the tRNA. *Bacillus subtilis* RNase Z is thought to use a two-metal (zinc in this instance) dependent catalytic mechanism with histidine residues in addition to aspartate residues used for metal-coordination (Li de la Sierra-Gallay et al., 2005). A 2006 paper describes an X-ray crystal structure of H65A *Bacillus subtilis* RNase Z bound to product tRNA that was thought possibly cleaved by contaminating RNases (Li de la Sierra-Gallay et al., 2006). In 2012, a WT *Bacillus subtilis* RNase Z pre-cleaved substrate complex was determined, and while authors describe use of 2′-O-methylation as a way to inhibit RNase Z cleavage, it is unclear to us how this would be achieved given that the enzyme is metal-dependent and the proposed mechanism is not thought to involve activation of the 2′–OH (Li de la Sierra-Gallay et al., 2005; Pellegrini et al., 2012). Possibly, as with the metal dependent RNase II-like *Mycoplasma genitalium* RNase R (*Mg*R) hydrolase, it is residues that guide the RNA to the active site, those in a "catalytic pocket," rather than residues more directly involved in the reaction, that influence 2′-O-methylation inhibition (Abula et al., 2021). Other RNase II homologs are not as inhibited by 2′O-methylation as *Mg*R (Abula et al., 2021). Yet for *Mg*R, it is proline 277, a residue not found in other RNase-II homologs that sterically inhibits 2′-O-methlyated RNA (Abula et al., 2021). Prolonged periods of incubation and higher concentrations of enzyme, conditions found in structural studies, did permit eventual *Mg*R degradation of 2′-O-methlyated RNA (Abula et al., 2021). Note that authors used a "catalytically inactive" D284A mutant to capture this RNase bound to unmodified RNAs (Table 3) as well as 2′-O-methylated (at position 3) 4-nt ssRNA (Table 2).

A second 2′–OH modification to trap RNase–RNA complexes pre-cleavage, albeit with a single found example, is that of 2′-fluorination (2′-F). Fully 2′-fluorinated RNA (FRNA) bound to reverse complement DNA prevents RNA cleavage by *Bacillus halodurans* RNase H (Pallan et al., 2016). This FRNA modification was used despite this RNase having a metal-dependent mechanism not thought to require a 2′–OH for cleavage; in fact, authors described fluorine as a better nucleophile than oxygen. Such FRNA/DNA hybrids still bind in the active site of RNase H making it possible to solve an RNase–FRNA/DNA substrate structure, although not perfectly and with three different occupancies for the majority of FRNA/DNA nucleotides due to what authors described as "slipping" (Table 2; Fig. 2C; (Pallan et al., 2016). Inhibition then, is thought to derive from a lack of metal ions observed in the active site of the complex structure; this is due to differences between 2′-O and 2′-F that caused structural differences of RNase-bound FRNA/DNA versus RNA/DNA duplexes (Pallan et al., 2016).

We are not certain why we did not find in our survey an RNase–RNA pre-cleavage complex involving an RNase that uses 2′-O activation bound to 2′-O-methyl or 2′-F modified substrates. Importantly, we think such modification would be preferrable to mimic the 3′-endo sugar pucker of RNA over the 2′-endo sugar pucker of DNA (Kawai et al., 1992; Malek-Adamian et al., 2018). Possibly, researchers have simply chosen what has worked for others, but if not, it is possibly that 2′-O-methylation and 2′-F sterically and/or electronically hinder nucleic acid binding. As evidence for this, 2′-F substitutions led to a disordered FRNA/DNA complex and slightly altered binding with RNase H (Pallan et al., 2016).

An additional method to inhibit acid-base RNA cleavage through substrate modification is to simply change the nucleotide positioned 5′ to the cut-site, to DNA. All identified examples that include this RNA to DNA modification are of RNases that use a 2′-O activation mechanism (Table 2), and therefore this modification appears to be the method-of-choice for this category of enzyme mechanisms. In the absence of a 2′–OH nucleophile, the cleavage reaction typically achieved by this oxygen is impossible. As seen in the following examples, modification of nucleotides from RNA to DNA is possible without altering the binding

Table 3
RNase–RNA structures determined using protein mutagenesis.

RNase	PBD ID	Substrate	Mutation (s)	Author
Homo sapiens AP endonuclease (APE1)	5DFJ	21 mer dsDNA with AP site at position 11 and a T:G mismatch 5′ to the AP site	E96Q & D210N	(Freudenthal et al., 2015)
Colwellia psychrerythraea 34H oligoribonuclease (ORN)	6A4E	2 linked uridines	D163A	(Lee et al., 2019)
Escherichia coli RNase II	2IX1	13 mer ssRNA	D209N	(Frazão et al., 2006)
Saccharomyces cerevisiae exosome core, Rrp44	2VNU	13 mer poly(A) RNA	D551N	(Lorentzen et al., 2008)
Aquifex aeolicus RNase III	1RC7	10 mer self-complementary dsRNA	E110K	(Blaszczyk et al., 2004)
	1YZ9	2 sets of, 11mer RNA forming 9 bp dsRNA with 2 nucleotides over hangs that form a duplex	E110Q	(Gan et al., 2005)
	1YYO	2, sets of self-complementary 12mer dsRNA	E110K	
Escherichia coli RNase E	5F6C	2 & 3 mer sRNA with 5′ monophosphates	D303R & D346R	(Bandyra et al., 2018)
	6G63	sRNA RprA		
Bacillus halodurans RNase H	1ZBI	Full complement 12 mer RNA/DNA hybrid	D132N	(Nowotny et al., 2005)
Thermovibrio ammonificans RNase H3	4PY5	Full complement 19mer RNA/DNA hybrid	D78N	(Figiel and Nowotny, 2014)
Thermotoga maritima RNase H2	3O3H	dsDNA with a single RNA 3′ to the scissile phosphate (manganese structure)	D107N	(Rychlik et al., 2010)
	3O3F	dsDNA with a single RNA 3′ to the scissile phosphate (magnesium structure)		
Escherichia virus T4 RNase H	2IHN	From input 18 and 24 mer strands, resolved region is of a dsDNA forked after 12 bp with 5 nucleotide overhangs	D132N	(Devos et al., 2007)
Human immunodeficiency virus 1 reverse transcriptase	4B3P	Hybrid of 29 mer DNA with 34 mer RNA	D498A	(Lapkouski et al., 2013)
	4B3Q	Hybrid of 25 mer DNA with 34 mer RNA	D498N	
Alkalihalobacillus halodurans RNase H	3TWH	6 mer RNA/DNA hybrid with 1 bp overhangs two Se atoms are present on DNA bases for phasing purposes	D132N	(Abdur et al., 2014)
Bacillus halodurans RNase H	3D0P	12 mer dsDNA	D132N	(Pallan and Egli, 2008)
Homo sapiens RNase H	2QKK	14-mer RNA/DNA hybrid	D210N	(Nowotny et al., 2007)
	2QK9	18-mer RNA/DNA hybrid		
	2QKB	20-mer RNA/DNA hybrid		
Thermus thermophilus RNase J	3T3N	15 mer 2′-O-CH_3 ssRNA	H77A	(Dorléans et al., 2011)
	3T3O	4 mer 2′-O-CH_3 ssRNA		
Influenza A virus PA subunit N-terminus (PA_N) endonuclease	6W7A	8 mer ssDNA	E119D	(Kumar et al., 2021)
Bovine viral diarrhea virus 1-CP7 glycoprotein Erns	4DW7	2 mer RNA	H32K	(Krey et al., 2012)
Leptotrichia buccalis Cas13a	5XWP	50 mer cRNA and 30 mer target RNA	R1048A, H1053A	(Liu et al., 2017)
Bacillus subtilis Mini-RNase III	6TNN	Precursor 23S rRNA as part of the *Bacillus subtilis* 50S ribosome	D23N	(Oerum et al., 2020)
Geobacillus stearothermophilus RNase M5	6TPQ	Precursor 5S rRNA of the *Bacillus subtilis* 50S ribosome	D58A	
Mycoplasma genitalium RNase R	7DOL	6 mer dsRNA with a 3′-ss overhang	D284A	(Abula et al., 2021)
	7DIC	9 mer ssRNA		

position of the substrate on the enzymes and can result in a realistic mimic of the pre-cleavage RNase–RNA substrate complex. *Thermos thermophilus* Cas6 (Table 2; Fig. 2D) was solved bound to an R1 stem-loop RNA substrate mimic with a single deoxyribonucleotide at G28, which typically harbors the 2′-O nucleophile necessary for cleavage (Niewoehner et al., 2014). The structure of *Bacillus subtilis* MazF (Table 2; PDB: 4MDX) bound to uncut UU*dU*ACAUAA has been determined; importantly the DNA did not prevent MazF from recognizing the UACAU cognate target sequence (Simanshu et al., 2013). This deoxy-inhibitory effect can also be achieved by using an entire strand of DNA, as in the structures of *E. coli* RNase I (Table 2; PDB: 2Z70), a non-sequence-specific RNase that acts as a scavenger in the cell, which was solved bound to uncut substrate mimic d(CGCGATCGCG) (Rodriguez et al., 2008), and *Lithobates catesbeiana* RNase A bound to uncut substrate mimic d(ACGA) (Table 2; PDB: 1 M07; (Leu et al., 2003).

A less common method of RNase inhibition that researchers have utilized for RNase–RNA pre-cleavage complex structure determination, is replacement of the scissile 5′-O with a CH_2 group, thus generating a 6′-C. The crystal structure of *Aspergillus oryzae* RNase T1, an enzyme with an acid-base mechanism, was solved bound in an unproductive manner to a guanylyl(3′-6′)-6′-deoxyhomouridine substrate (Table 2; Fig. 2E; (Arni et al., 1999). While the 5′-O typically has an electron withdrawing effect on the scissile phosphorous making it a better electrophile during the RNase cleavage reaction, a CH_2 group in that position creates a phosphonate; this reduces the availability of the scissile phosphorous as an electrophile and likely contributes to its uncleavable nature.

RNA base(s) sequence change

A different way to form RNase–RNA pre-cleavage complexes is to alter the base compositions, i.e., the sequence, of cognate RNA substrate. Changing RNA sequences in general can have a number of effects that include altering secondary and tertiary structure, especially if a change disrupts an intra- or inter-strand base-pairing interaction. Regarding RNase recognition, altered local RNA structure might prevent proper active site orientation of constituents required for RNA cleavage, while preserving structure elsewhere for proper binding. While there are examples of ribozymes utilizing base components directly in the cleavage reaction (Golden, 2011; Ward et al., 2014; Wilcox et al., 2011; Zhao et al., 2005), in proteins these roles have often if not always been replaced by functional groups of amino acid residues. If bases of an RNA substrate bound to an RNase happen to be important for active site chemistry and mimic what we know of ribozymes in any way, the roles involved in catalysis could include i) properly orienting other active site atoms, ii) altering the local pKa of necessary active site functional groups, and iii) recruiting metal co-factors. Largely, however, we expect mutating bases of cognate RNase targets to perturb either the RNA structure and/or proper recognition and positioning required for RNA

cleavage chemistry to occur.

As part of being an RNA-templated DNA polymerase, HIV-I reverse transcriptase (RT) accommodates an RNA/DNA chimera in the active site of the synthesizing DNA polymerase, yet also has a modular attached RNase H domain responsible for cleaving RNA as it is bound to DNA. Tian et al. (Tian et al., 2018) utilized an extensive list of modifications and strategies to achieve their goal of capturing the HIV-I RT complex with the RNase H domain bound to an RNA/DNA duplex substrate in a properly positioned pre-cleavage state (Table 2; Fig. 3A). Earlier HIV-1 RT complex-containing structures showed that the RNA/DNA could bind, but placed the RNA too far away from the active site for cleavage (Tian et al., 2018). Prior work showed that the RNA/DNA helix required bending between the DNAP and RNase H domains to position the scissile phosphate into the active site of the RNase H domain and explained why RNA was not cleaved with sequences that did not permit this bending and that prevented substrate from properly entering the active site. By altering the sequence of RNA (and paired DNA), the RNA/DNA duplex was then able to bend properly to position the RNA strand for RNA cleavage, however, this cleavage was inhibited by the incorporation of inhibitory Ca^{2+} over reactive Mg^{2+} ions.

Tian et al. had to first consider the polymerase portion of the heterodimer complex, and how to disfavor the activity and RNA/DNA binding of this domain, and therefore used an abasic site, which has backbone composition but lacks a base that in this instance is a template for what would be the + 1 DNA nucleotide addition if the polymerase were active. Additionally, and to be described in the mutagenesis section of this review, the authors also used an NNRTI inhibitor of the polymerase domain to favor RNA/DNA bound in a state for RNase H cleavage. To improve crystal diffraction resolution, the authors manipulated and tested different lengths of DNA and RNA overhangs of the RNA/DNA duplex; these changes not only altered resolution and crystal packing, but also the placement of substrate in the complex. Also for crystallization purposes, the authors chose to artificially introduce a nick by annealing two separate RNA strands to the DNA strand. Most important to this section of our review here, was the base mutations the authors used upstream to the cleavage site. The authors performed biochemical cleavage reaction experiments and combined with previous published knowledge, generated preferred and unpreferred cleavage substrates for crystallization. Using the information that UA −5/-4 relative to the cut-site was unfavored, and GU preferred, while A was not

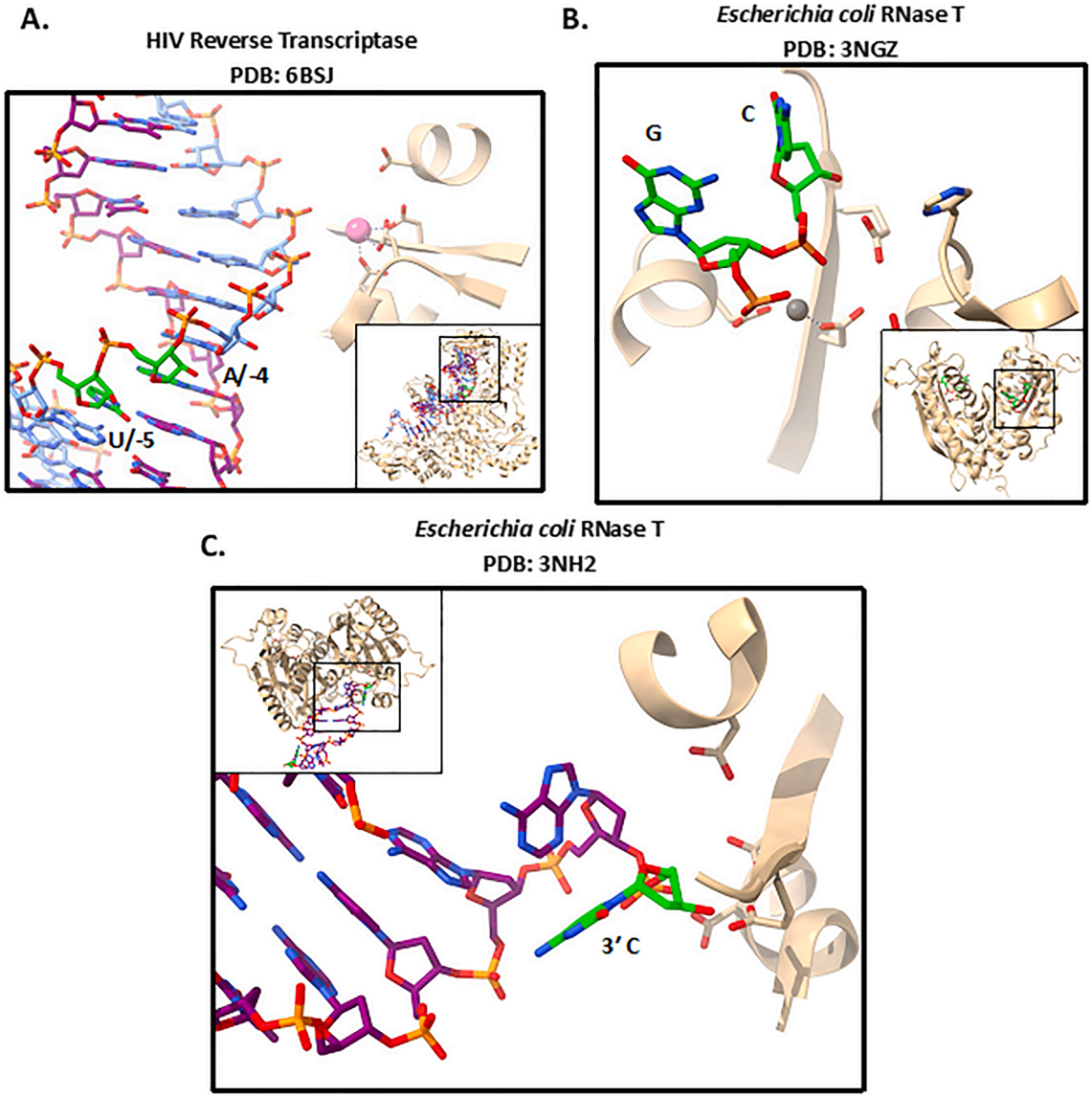

Fig. 3. RNase–pre-cleavage substrate complexes that incorporate base substitutions or manipulation. A.) 2.89 Å resolution X-ray crystal structure of HIV-1 RT bound to an RNA/DNA hybrid. B.) 2.1 Å resolution X-ray crystal structure of *Escherichia coli* RNase T bound to a d(GC) dinucleotide with one metal bound in the active site. C.) 2.3 Å resolution X-ray crystal structure of *Escherichia coli* RNase T bound to a dsDNA with two nt overhangs ending with a 3′ C residue.

favored at the −2 position, Tian et al. determined a structure where a preferred sequence for cleavage was used and found bound in the active site properly to mimic a pre-cleavage state.

Multiple nucleotide preferences determine cleavage-site recognition by the HIV-1 and M−MuLV RNase H (Schultz et al., 2010) As part of the viral life cycle, Tian et al. knew that polypurine at the cleavage site prevented HIV-1 RT RNase H cleavage, especially as these regions remain intact to be used as primers for DNA polymerization by this enzyme. By changing the sequence of the region near the cleavage site they were able to capture an X-ray crystal ("crystal 4") structure complex that revealed a > 4 Å scissile phosphate displacement away from the position favored for catalysis; the RNA/DNA duplex was also comparatively straighter especially relative to the structure with substrate in position for catalysis, and this caused extension of the HIV-RT. Since RNase H enzymes cleave RNA by recognizing DNA/RNA interstrand hybrid helical structures, sequences that alter helical structure therefore perturb proper positioning of the scissile phosphate in the active site for cleavage. DNA-RNA chimeras typically adopt a more A-like helical form like that of RNA double-helices, unlike B-form DNA double-helices, yet can adopt intermediate conformations between the two forms by varying purine and pyrimidine composition (Gyi et al., 1996; Gyi et al., 1998). Tian et. al (2018) note in their work the numerous nucleic acid constructs they had to test before arriving at their desired complex and this perfectly illustrates the rationally designed path they used, utilizing multiple techniques simultaneously, to achieve their ultimate goal.

The next example of the utilization of selective bases to inhibit cleavage derives from natural inhibition of RNase T (also discussed in the pH manipulation section) activity by inclusion of C residues at the 3′ end of nucleic acid substrates, called the "C effect"(Hsiao et al., 2011). Hsiao et al. (Hsiao et al., 2011) determined X-ray crystal structures of RNase T bound to DNA substrates with inhibitory terminal C residues to elucidate how these residues inhibit substrate cleavage (Table 2; Fig. 3B, C). In this case, it is a natural occurrence that leads to the ability to capture an RNase–DNA (likely mimicking RNA) pre-cleavage complex. This, and the example above, exemplify the importance of understanding sequence preference and specificity biochemically prior to designing structural studies. The authors found that a 3′ C residue nucleobase is recognized specifically by an E73 interaction, and does not stack with F29 as when other bases are at this position; these interactions are associated with a conformational change where an activating base H181 is no longer in proper position for catalysis, metal A is not bound (metal B is modeled in the "non-preferred" 5′-GC-3′ substrate structure only), and the scissile phosphate is 1.43 Å away from a preferred catalytic position when two metals are bound (Fig. 3B). This work perfectly illustrates the "effect" that base components can have on trapping RNase–DNA/RNA pre-cleavage complexes. The authors then went on to determine a structure of RNase T in complex with a dsDNA substrate (Fig. 3C); here, a 5′-d(TTACAAC)-3′ sequence was used that in theory should produce a single 3′ C base overhang on either side of a duplex formed from annealing two identical strands, however they found that due to the weak A–T interaction, rather two bases were in the overhangs and the 3′ C again interacted as in the prior complex. Here again, base composition has an effect on achieving capture of a nucleic acid substrate bound to the active site of an RNase in a pre-cleavage state. Interestingly, RNase T in complex with single-stranded, as well as double stranded DNA utilized the same 5′-d(TTACAAC)-3 substrate, however crystals had different space groups, illustrating the effects of crystallization on successful structural studies in capturing RNase pre-cleavage complexes.

Protein mutagenesis

Site-directed mutagenesis is one of the most powerful tools in protein biology; it is commonly used by enzymologists and structural biologists to identify important amino acid residues. In the context of solving RNase protein–RNA pre-cleavage substrate-bound complexes, mutation sites are identified that disturb the catalytic potential of the protein. The amino acids targeted for mutation can be identified by existing experimental knowledge, and prediction through homology modeling and/or sequence alignments (Ahola et al., 2004; Baek et al., 2021; Jumper et al., 2021). Typically, three or more RNase active site aspartate and/or glutamate carboxy groups coordinate two divalent metal ions, which are often Mg^{2+} (Sosunov et al., 2003); these negatively charged side chains can also indirectly coordinate metals through a bound water intermediary. There are several helpful consequences provided by mutation of key active site residues in regards to inhibiting RNase activity: i) disrupting all catalytic metal binding while maintaining the natural RNA binding mode; ii) disrupting some, but not all, catalytic metal binding while maintaining the natural RNA binding mode; iii) displacement of divalent metals within the active site so that catalysis is impossible while maintaining the natural RNA binding mode; iv) disrupting catalytic metal binding with alteration in RNA binding mode; and v) alteration of catalytic residues important for acid-base mechanisms. Below we discuss how mutations affect RNase activity inhibition and the resulting RNase–RNA complex structures that were able to be determined.

Protein mutagenesis causing metals to be absent in the structure of the RNase active site

Although *Homo sapiens* APE1 was solved bound to 21 mer dsDNA versus dsRNA, and also with an AP site at position 11 and a T:G mismatch 5′ to the AP site (Table 3; Fig. 4A; (Freudenthal et al., 2015), mammalian APE1 has been shown to cleave RNA (Antoniali et al., 2017; Kim et al., 2010), and methods used in its inactivation are identical to those used in RNases. Two active site mutations, E96Q and D210N, inactivated the enzyme. Notice that both residues mutated are carboxylic acids; this will be a common theme in this section and is of great importance due to the role of acidic residues in metal binding. The functional difference between E,D and Q,N, respectively, is a nitrogen in place of one of the carboxylic oxygens. The result of these mutations in APE1 is a hydrogen bonding arrangement between Q96, N68 and N210 (represented by black dashed lines in Fig. 4A). This arrangement rotates carboxylic oxygen away from the metal binding pocket resulting in the absence of divalent metal ions in the active site (Freudenthal et al., 2015).

Inactivating RNases by mutagenesis of conserved residues also provides biochemical information about the enzyme in question when compared with the wild-type (WT) form. In combination with mutant RNase–RNA complex structure elucidation, this creates a potent method for studying RNase mechanisms from a structural point of view. *Colwellia psychrerythraea* oligoribonuclease (CpsORN) is an exoribonuclease involved in 3′-5′ mRNA processing. *Colwellia psychrerythraea* 34H is a bacterium which lives deep in sea ice and has been shown to have measurable metabolic activity at a temperature as low as −196 °C (Junge et al., 2006); for this reason it may be difficult to use the temperature snapshots method (discussed below) on RNases from this and other psychrophilic organisms. The X-ray crystal structures of RNase activity inhibited CpsORN D163A were solved bound to different cleavable RNA or RNA-like substrates including 5′-O-[(S)-hydroxy(4-nitrophenoxy)phosphoryl]thymidine (*p*NP-TMP; PDB: 6A4D) and a r (U_5) strand, although only two uridines were modeled (Table 3; PDB: 6A4E; (Lee et al., 2019). Again, the mutation is of an amino acid bearing a carboxylic acid, however in this example it is replaced with an alanine, completely removing oxygens and the metal coordination they can provide. This is a common strategy as alanine bares only a methyl R group and is commonly used in "alanine scanning" to identify important amino acid residues by removing the majority of other R-groups while providing increased rigidity as opposed to a glycine replacement. A structural alignment between the unliganded CpsORN WT (PDB: 6A4A) and *p*NP-TMP bound CpsORN D163A form revealed a 0.503 Å root mean square deviation (RMSD); the conformation shift is attributed to the lack

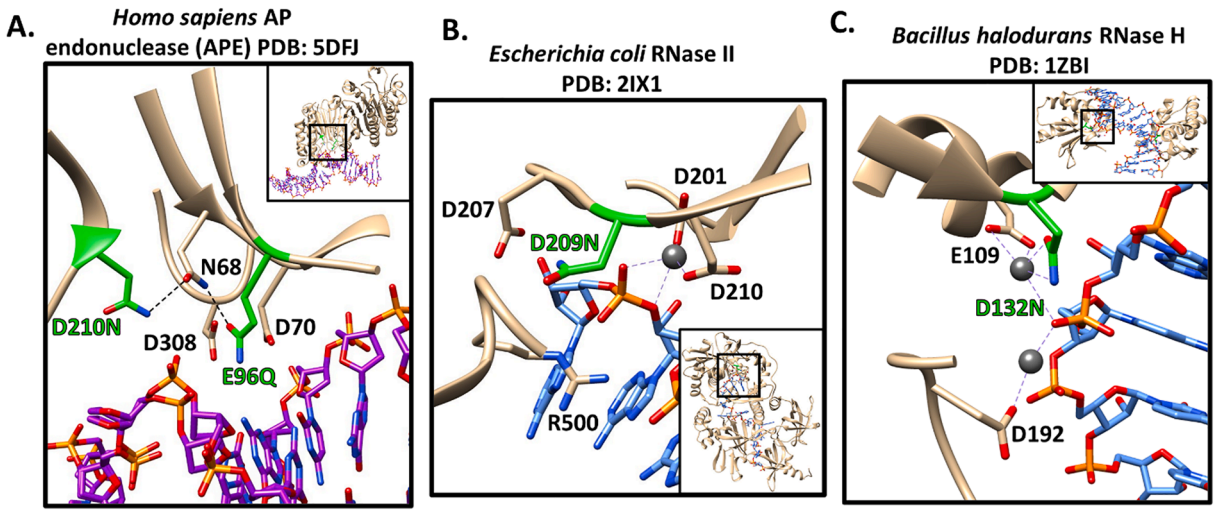

Fig. 4. Examples of RNase(mutant)–RNA pre-cleavage complexes with varying numbers of catalytic metals present. A.) 1.85 Å resolution X-ray crystal structure of *Homo sapiens* AP endonuclease 1 E96Q/D210 bound to DNA. B.) 2.74 Å resolution X-ray crystal structure of *Escherichia coli* RNase II D209N bound to one Mg^{2+}. C.) 1.85 Å resolution X-ray crystal structure of *Bacillus halodurans* RNase H D132N bound to RNA and two Mg^{2+}.

of a metal ion in the D163A form, indicating that naturally, D163 is involved in metal ion binding that brings the enzyme into a catalytically active conformation.

In the first reported structure of a flap endonuclease bound to its substrate, Escherichia virus T4 RNase H D132N was solved bound to 18/24 forked DNA where the resolved region is of a dsDNA forked after 12 bp with 5 nucleotide overhangs (Table 3; PDB: 2IHN; (Devos et al., 2007). D132N was shown to be an inactivating mutant (Bhagwat et al., 1997). Ethylenediaminetetraacetic acid (EDTA) was used to remove metals. Though there are not metals present due to EDTA, it is likely that the D132N mutant would have disrupted the natural binding mode of magnesium in the active site regardless, but it is difficult to say to what extent without the metals free in solution.

The structure of *Bacillus halodurans* RNase H D132N was solved bound to 12 mer dsDNA (Table 3; PDB: 3D0P; (Pallan and Egli, 2008). D132N is a deactivating mutation but the lack of bound metals was more so attributed to the lack of 2′-O in the DNA substrate that causes conformational changes in other active site residues and small differences in coordination of the substrate. The end effect is thought to be steric and electrostatic chemistry alterations that alter the metal binding site (Pallan and Egli, 2008).

The catalytic domain of *Homo sapiens* RNase H D210N was solved bound to 14, 18, and 20 mer RNA/DNA hybrids (Table 3; PDBs: 2QKK, 2QK9, and 2QKB; (Nowotny et al., 2007). D210N was selected by Nowotny et. al. for crystallization due to its lack of activity in the presence of both Mg^{2+} and Mn^{2+}. RNA/DNA and dsRNA binding with the D210N mutant was confirmed with an electromobility shift assay (Nowotny et al., 2007). Sedimentation equilibrium experiments proved that human RNase H binds RNA/DNA hybrids preferentially over dsRNA. Subsequently, an RNA/DNA hybrid was used in structure determination (Nowotny et al., 2007).

HIV-1 reverse transcriptase (HIV-1 RT) contains both a DNA polymerase active site and an RNase H active site in separate locations (Sarafianos et al., 2009). In the X-ray crystal structures with PDBs 4B3P and 4B3Q, D498 was mutated to eliminate RNase H activity; in the latter structure a non-nucleoside reverse transcriptase inhibitor (NNRTI) was used to inactivate the DNA polymerase activity (Table 3; PDB: 4B3P & 4B3Q;(Lapkouski et al., 2013). Since both the RT domain and the RNase H domain can bind to an RNA/DNA hybrid, an NNRTI bound to the RT domain occluded, through forming an open conformation, the RNA/DNA hybrid from binding to the polymerase, and therefore favored binding to the RNase domain. This highlights the necessity for researchers to first understand as much as possible about the context and mechanisms of RNases before choosing an appropriate RNase inhibiting technique for structural studies.

Protein mutagenesis causing one of two metals to be modeled/present in the RNase active site

Yeast Rrp44 is the nuclease subunit of the yeast exosome which is responsible for cleaving ssRNA (Lorentzen et al., 2008). The structure of Rrp44 (242–1001) D551N was determined bound to 13 mer poly(A) ssRNA (Table 3; PDB: 2VNU; (Lorentzen et al., 2008). The D551N mutation eliminates nuclease activity of Rrp44; only one metal is bound in the active site, and this can likely be attributed to electronic differences of WT compared to the D551N mutant, as well as the positioning of N551, of which the functional group was modeled facing away from the metal binding pocket.

RNase II, the bacterial homolog of Rrp44, contains three RNA binding domains and an “RNB” domain (named for the *rnb* gene that encodes RNase II that confers RNase activity (Frazão et al., 2006). RNase II-like proteins are fundamental actors in RNA maturation of most organisms; not only are eukaryotic homologs subunits in the exosome but individually bacterial RNase II can catalyze RNA degradation reactions as a standalone enzyme (Frazão et al., 2006; Matos et al., 2014). The X-ray crystal structure of an RNase II D209N–13 mer ssRNA complex bound with a single Mg^{2+} in the active site has been determined (Table 3; Fig. 4B; Frazão et al., 2006). Prior to this, protein mutagenesis was used to predict the important residues and enzymatic mechanism of RNase II (Amblar and Arraiano, 2005). While WT RNase II readily cleaved SL9A and malE-malF mRNAs into multiple products, a D209N mutant in the RNB domain showed zero activity for either substrate (Amblar and Arraiano, 2005). Gel retardation assays showed that the D209N mutant had comparable RNA binding affinity to WT, indicating that D209 is either involved in metal binding necessary for catalysis or possibly, since activity could not be rescued by increasing the Mg^{2+} concentration, acts as a primary base for hydrolysis and not with binding (Amblar and Arraiano, 2005). An RNase II cleavage mechanism was put forth using this structure, as well as comparison with the RNase mechanism knowledge of RNase H (Nowotny et al., 2005), which has a similar active site. Active site superimposition of RNase H showed that if D209 would have been present (rather than the N209 mutant residue) that it along with D207 would be in position to coordinate a second Mg^{2+} for the cleavage reaction to then occur (Frazão et al., 2006). Determining the X-ray crystal structure of the RNase II D209N–13 mer ssRNA complex was the keystone piece of information, along with the previously

known RNase H mechanism (Nowotny et al., 2005), that supported existing biochemical evidence (Amblar and Arraiano, 2005) to explain an RNase II two-metal catalyzed RNA degradation mechanism.

RNase H family member *Thermovibrio ammonificans* RNase H3 D78N was solved bound to a 19 mer RNA/DNA hybrid (Table 3; PDB: 4PY5; (Figiel and Nowotny, 2014). One of two metals is missing in this structure and this is attributed to the D78N mutation. Though N78 is a ligand of the metal that is present, it indirectly affects the ability of the second metal ion to bind in the metal binding pocket (Figiel and Nowotny, 2014). Interestingly one of the other active site residues, D180, shows double occupancy where each sidechain is rotated about 180° relative to one another suggesting this second metal when bound is responsible for coordinating and stabilizing D180 for RNase activity. In the X-ray crystal structure of Influenza A PA_N endonuclease bound to ssDNA (Table 3), only one of the two metals were modeled bound in the active site when DNA was used as the substrate and in the context of a PA_N E119D mutant that the authors describe as "catalytically impaired" (Kumar et al., 2021). The DNA substrate, which is known to be cleaved by this enzyme, was not cleaved, and was positioned out of register (PDB: 6W7A). This E119D mutation is interesting given that glutamic acid and aspartic acid have similar carboxyl R-groups, despite aspartic acid being shorter; D119 does interact with one of the two metals (here Mn^{2+}), yet the position of the substrate phosphates is not positioned as expected for cleavage. While the inhibitory E119D mutation could be considered important to capturing this pre-cleavage state, the authors also suggest other possibilities that include the fact that this RNase activity is typically involved in "cap snatching" of mRNA and therefore involves more residues 5′ to the cut site, combined with an RNA substrate preference over DNA.

Protein mutagenesis causing two metals to be modeled/present in the RNase active site

Typically, two-metals bound in the active site of RNases that use a two-metal catalytic mechanism would suggest the occurrence of RNase cleavage and an inherent inability to then capture an RNase–RNA pre-cleavage complex structure (since chemistry would occur). As we discuss next however, there are examples of determined RNase–RNA complex structures containing intact RNA despite the presence of two metals in the active site. Some RNase H family members can cleave dsRNA and RNA/DNA hybrids to remove primers from Okazaki fragments, and are present in both eukaryotic and prokaryotic organisms (Cerritelli and Crouch, 2009). A *Bacillus halodurans* RNase H with active site mutations at E109 or D132 were found incapable of cleaving a 12 mer RNA/DNA substrate; a D132N *Bacillus halodurans* RNase H mutant enhanced binding of this 12 mer RNA/DNA substrate and also made possible capturing this pre-cleavage complex for X-ray crystal structure determination (Table 3; Fig. 4C;(Nowotny et al., 2005). Interestingly, while both metals were found present in this structure, D132N changed positioning of a metal within the active site rendering the active site non-catalytic.

Both metals, i.e. two magnesiums in one structure (Table 3; PDB: 3O3F) and two manganese in another (Table 3; PDB: 3O3H), were modeled in the active site of the X-ray crystal structure of *Thermotoga maritima* RNase H2 D107N bound to a dsDNA that had single RNA nucleotide positioned 3′ to the scissile phosphate (Rychlik et al., 2010). In the structure, one metal occupies the A site while the other, instead of occupying the normal B site, occupies what is known as the C site based on a structure solved with 3 calcium ions (PDB: 3O3G) from the same publication (we will discuss this further in our *Metal Ion Chelation and Replacement* section below). The D107N mutant was attributed to this shift in metal placement, and residues D18 and E19 show double occupancy that may be a result of the altered metal binding state.

A third example of two metals modeled in an RNase active site when bound to RNA and prior to cleavage includes the X-ray crystal structure of *Alkalihalobacillus halodurans* RNase H D132N bound to a 6 mer RNA/DNA hybrid with selenium derivatized DNA for multi-wavelength anomalous dispersion phasing (Table 3; PDB: 3TWH; (Abdur et al., 2014). A direct reason for lack of activity in D132N was not given by the authors, but it can likely be attributed to the effect of N132 on metal binding. We performed a structural alignment (RMSD of 0.172 Å) between this structure and that of the WT–6 mer RNA/DNA hybrid that possesses two Mg^{2+} ions in the active site (PDB: 6DMV; (Samara and Yang, 2018); (discussed further in the temperature snapshots section). This alignment revealed that D132 (i.e. WT) and N132 (i.e. mutant) were modeled in the same orientation (not shown), so it is likely that it is electronic differences of O compared to N that cause the catalytic metal to bind in a different position (a 0.507 Å shift in position for this coordinated metal) and therefore inhibit cleavage activity.

Protein mutagenesis causing RNA to bind in an alternate binding position

Mutations designed to inhibit metal binding can also affect catalytic activity by changing overall conformation, especially considering that RNases can be domains or subunits within a larger macromolecular context. By cleaving dsRNAs, RNase III family members perform a number of cellular functions involving RNA maturation and regulation, for example as part of RNA interference mechanisms (Court et al., 2013). RNAse III can sequester dsRNA without cleaving it to perform a regulatory function as well, and this gives rise to the ability to capture a "nonenzymatic" complex bound to intact dsRNA and catalytic metals (Blaszczyk et al., 2004; Court et al., 2013). An example of this is with an X-ray crystal structure containing Aquifex aeolicus RNase III (Aa-RNase III) (Table 3; Fig. 5B), which consists of two structural domains connected by a flexible linker, a double stranded RNA binding domain (dsRBD) and a catalytic endonuclease domain (endoND) (Blaszczyk et al., 2004). In this structure Aa-RNase III residue E110 resides in each monomer of the dimerized endoND, and along with two other negatively charged residues binds a divalent metal ion. E110K disrupts metal binding presumably through repulsion due to the change in charge of this residue and renders this RNase catalytically inactive. The absence of a positively charged metal ion leaves the negatively charged pocket including E40, D44, D107 and K110 residues exposed, inhibiting RNA binding and resulting in an alternative dsRNA binding form and conformational change of the position of the two dsRBDs of the dimer (Blaszczyk et al., 2004). In the form for RNA cleavage, one dsRNA is positioned between two dsRBDs and the active site, but in the "nonenzymatic" binding form, each dsRBD binds a different dsRNA, neither of which resides in the "catalytic valley" (Blaszczyk et al., 2004). This is an example of a mutation that caused a significant conformational change to the protein and inhibited binding of the RNA to the active site but still provided useful functional molecular information. This work was expanded upon using different dsRNAs, and E110Q and E110K mutant Aa-RNase III proteins to generate structures and models that depict conformational changes and alternative dsRNA binding arrangements (Table 3; PDBs: 1YYO & 1YZ9; (Gan et al., 2005). These examples illustrate that it is possible to study RNA interactions with the non-RNase domains of multidomain RNases by inhibiting the RNase domain.

RNase E is one component of a multi-protein complex called the degradosome where it cleaves and processes multiple forms of RNA; the N-terminal domain (NTD) contributes catalytic activity to RNase E while the C-terminal domain is mostly structural, for protein–protein binding within the degradosome (Bandyra et al., 2018). The NTD contains RNase H and DNase I like regions and oligomerizes to form a quaternary organization for substrate cleavage. Catalytic activity is increased in the presence of a 5′ monophosphate due to an increase in K_M for these substrates (Kime et al., 2010; Mackie, 1998). Additionally, RNase E can bind dsRNA regions within cognate RNA targets. Revealing the difference of these RNase E RNA recognition modes and how they may even work in tandem, the X-ray crystal structures of RNase E NTD D303R, D346R in complex with RNA MicC (12 mer) fused to an *ompD* fragment RNA (Table 3; PDB: 5F6C) and with full length (106 mer) small

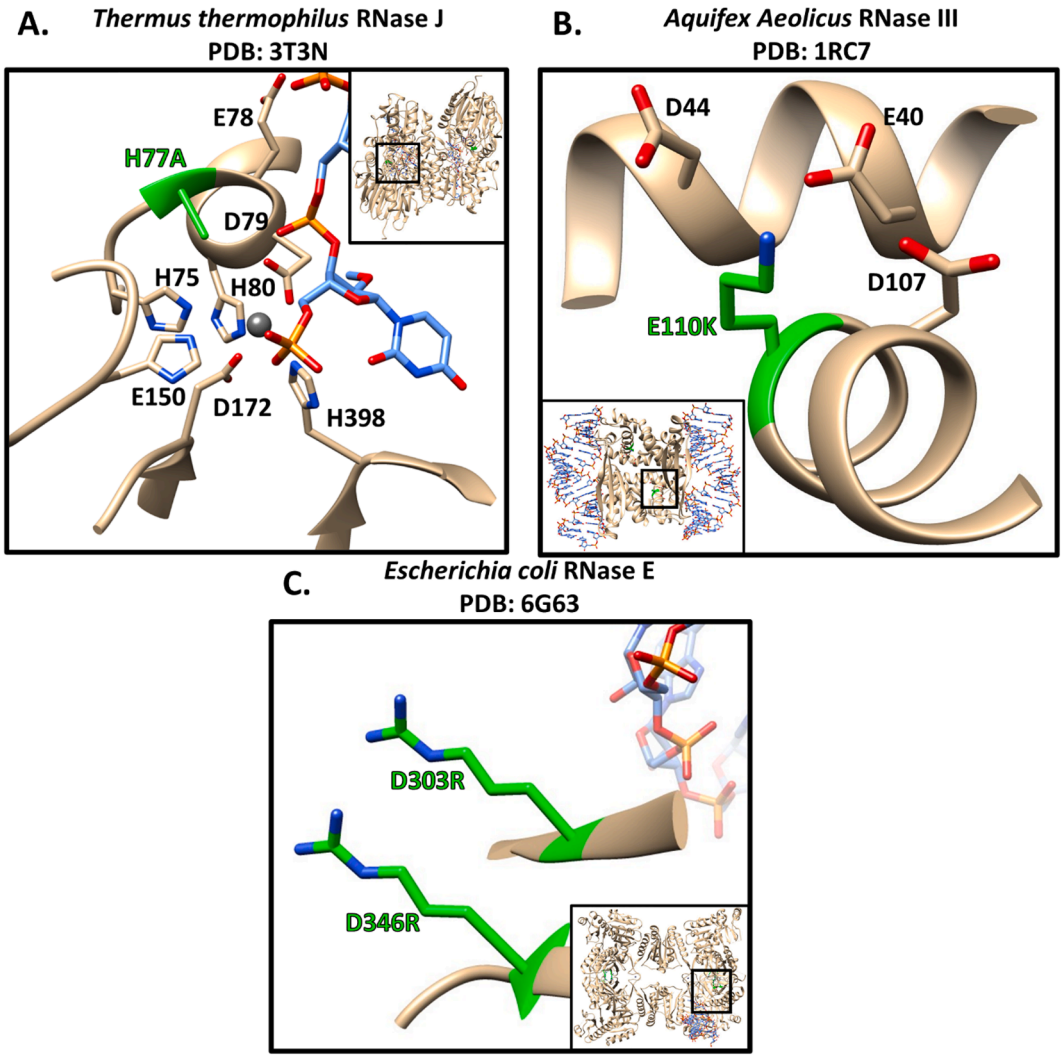

Fig. 5. RNase–pre-cleavage substrate and/or substrate-mimic complexes that utilize protein mutagenesis methods for inhibition with RNA bound in alternate binding site. A.) 3.09 Å resolution X-ray crystal structure of *Thermus thermophilus* HB27 RNase J bound to RNA with one Zn^{2+}. B.) 2.15 Å resolution X-ray crystal structure of *Aquifex Aeolicus* RNase III E110K bound to RNA. C.) 3.95 Å resolution X-ray crystal structure of *Escherichia coli* RNase E bound to RNA.

regulatory RNA (sRNA) RprA (Table 3; Fig. 5C) were determined (Bandyra et al., 2018). RNase E D303R and D346R mutations were used to deactivate cleavage activity, along with the use of 2′O-methylated MicC fused to *ompD* fragment RNA nucleotides (nts) + 82 and + 83 downstream from the translation start site (Bandyra et al., 2018). In each determined structure, only a minimal region of RNA was resolved and modeled, and no RNA in the cleavage active site. The MicC bound structure revealed a 5′ binding surface, and the RprA bound structure revealed a binding surface for dsRNA that was modeled as an A_{12}:U_{11} duplex and not of the true dsRNA sequence, given the low resolution (3.95 Å resolution). RNA was not cleaved in either structure as determined experimentally and the conformation was more "open" than that of a "closed" stated known to form when bound to RNA substrate, however more "closed" than the apo form (Callaghan et al., 2005; Koslover et al., 2008). These studies revealed how mutations, at least in part, can be used to structurally reveal important and functionally relevant alternative RNase–RNA binding modes (Bandyra et al., 2018).

Another example of protein mutagenesis permitting capture of an RNase bound to uncleaved RNA that is displaced from the active site is the X-ray crystal structure of *Thermus thermophilus* RNase J H77A bound to 15 mer 2′-O-CH3 ssRNA (Table 3; Fig. 5A) and 4 mer 2′-O-CH3 ssRNA (Table 3; PDB: 3T3O; (Dorléans et al., 2011). In the former, only one of two catalytic Zn^{2+} metal ions is present in the active site. Though it is unclear if the mutant H77A is directly responsible for the lack of a second ion or if it is the modified RNA, the lack of a second ion is responsible for the lack of activity. The scissile phosphate is displaced from the active site as it resides 6.7 Å from the lone Zn^{2+} and is unable to be cleaved at that distance (Dorléans et al., 2011).

Reconstituting pre-mature ribosomal complexes containing bound RNases in pre-cleavage states for cryo-EM structure determination

The work by Oreum et al. published in 2020 (Oerum et al., 2020) is a great example of the power of point mutations within RNases to assemble pre-cleavage complexes for structure determination, as well as the benefits of cryo-EM for such studies. In their study, they combined genetic engineering, recombinant mutant RNase production, X-ray crystallography, and cryo-EM techniques to elucidate Mini-RNase III bound to pre-5S RNA, and RNase 5 bound to a pre-23S rRNA, both within the context of the otherwise 50S *Bacillus subtilis* ribosomal subunit (Table 3). Each of these RNases binds and cleaves dsRNA for 50S rRNA maturation and these structures give great insight to these processes. Respective premature 50S ribosomal subunits were generated by knockouts in *Bacillus subtilis* of proteins for respective maturation pathways, leaving uncleaved dsRNA substrate targets intact, and then recombinant wT enzymes were added back. Recombinantly produced

D23N Mini-RNase III and D58A M5 RNase, each with a mutation that disrupted the two-metal catalytic active sites, were then combined with the appropriate pre-mature 50S ribosome for cryo-EM analysis. To overcome the problem of weak binding affinity, a possible inherent problem with mutant proteins, and therefore poor electron density for cryo-EM modeling, the ratio of 50 s ribosomes to RNases was increased to 1:210. In the final models, one metal was modeled in each active site of the bound dimer Mini-RNase III and no metals for bound monomer M5. Each RNase was then able to be modeled bound to the dsRNA substrates they recognize while maintaining a low enough background that included unbound RNase. In the case of M5, X-ray crystal structure determination of an N-terminal portion, and separately a C-terminal portion, were used in the modeling of the cryo-EM structure, where the cryo-EM data permitted modeling of a linking region between these two regions in the M5 protein.

Acid base catalysis

Mutagenesis of active site residues in RNases with acid-base catalytic mechanisms also been successfully used to form pre-cleavage complexes like with Cas13a that utilizes activation of an RNA 2′OH that is 5′ to the cut site (Knott et al., 2017). *Leptotrichia buccalis* Cas13a with R1048A and H1053A mutations were used to capture and determine the X-ray crystal structure of this RNase bound to 50 mer cRNA and 30 mer target RNA (Table 3; Fig. 6C; (Liu et al., 2017). Cas13a contains two Higher Eukaryotes and Prokaryotes Nucleotide-binding (HEPN) domains which fold together to form an active site with R1048 and H1053 as catalytically important residues of the HEPN2 domain that when mutated to alanine disrupts the otherwise acid-base chemistry utilized by Cas13a to cleave target RNA. Authors determined through these mutations that binding of Cas13a to target RNA brought catalytic residues of the two HEPN domains closer than when not bound to target RNA, and this activates nuclease activity important for collateral ssRNA cleavage (Liu et al., 2017). In the case of the determined X-ray crystal structure of

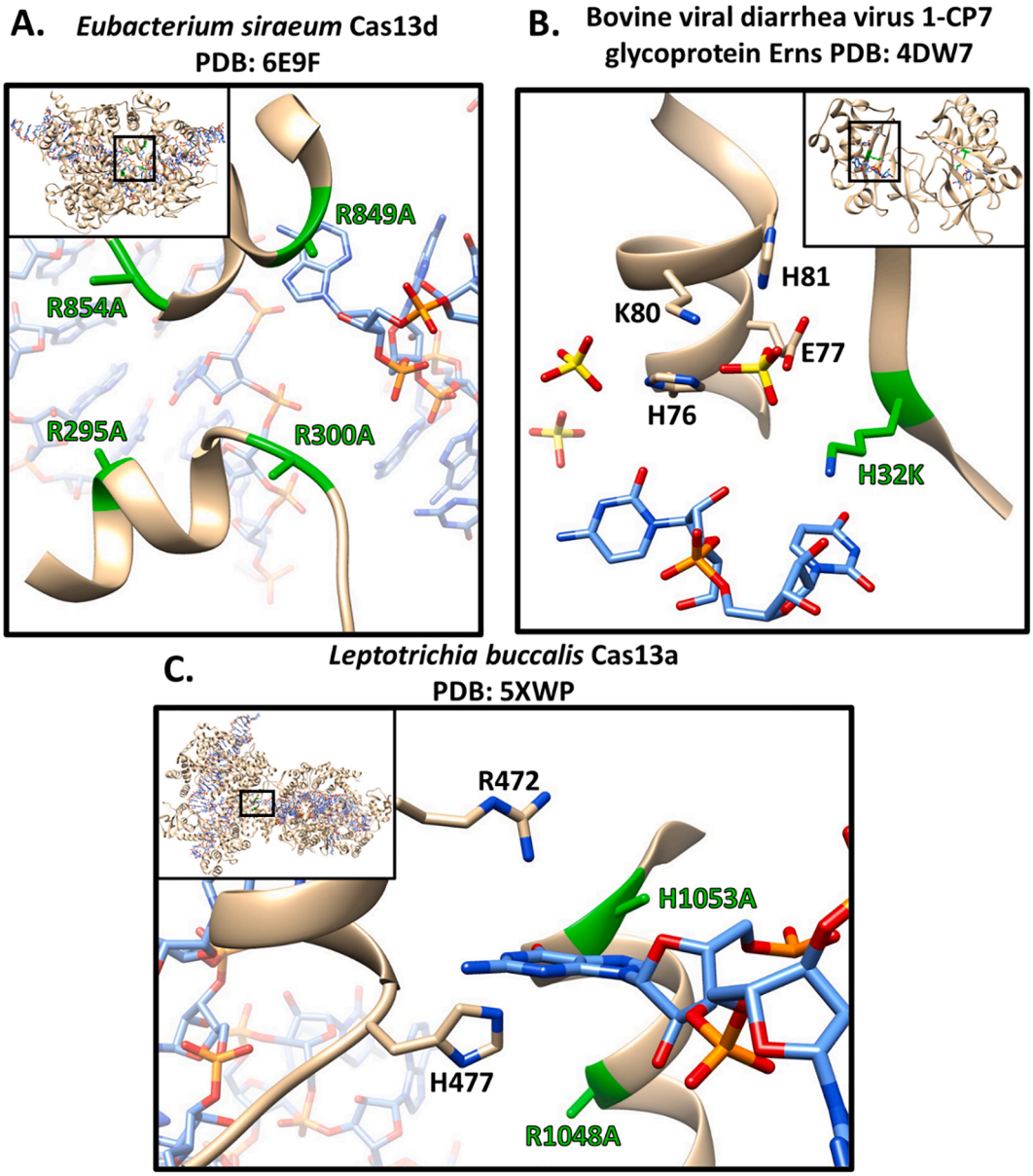

Fig. 6. Examples of RNase–pre-cleavage substrate and/or substrate-mimic complex structures that utilized protein mutagenesis methods for inhibition of an acid-base mechanism. A.) 3.30 Å resolution X-ray crystal structure of *Eubacterium siraeum* Cas13d bound to RNA. B.) 3.08 Å resolution X-ray crystal structure of *Bovine viral diarrhea virus* glycoprotein Erns in complex with RNA. C.) 3.09 Å resolution X-ray crystal structure of *Leptotrichia buccalis* Cas13a bound to RNA.

Eubacterium siraeum Cas13d bound to 52 mer cRNA and intact 27 mer target RNA (Table 3; Fig. 6B), active site mutations R295A, H300A, R849A, and H854A were similarly used to disrupt acid-base catalysis (Zhang et al., 2018), although here mutated residues were active site residues within both HEPN domains instead of just one.

Another example of mutations utilized to disrupt acid-base catalysis to trap and determine an RNase–pre-cleavage RNA complex involves glycoprotein Erns, which is a T2 like RNase that resides on the surface of bovine viral diarrhea virus 1-CP7 and cuts single and double stranded RNA (Iqbal et al., 2004; Schneider et al., 1993; Yi et al., 2012). In the structure of the inactive Erns mutant H32K bound to 2 mer RNA (Table 3; Fig. 6B (Krey et al., 2012) the RNA is bound in an RNA binding pocket outside of the active site. This is a result of the active site being occupied by sulfate ions, which chemically mimic the phosphate backbone of RNA and directly compete for active site occupancy (Krey et al., 2012). H32 in WT Erns would normally act as a proton donor for product release, however K32 deactivates the enzyme by precluding this process.

Crystallization condition manipulation

Metal ion chelation and replacement

Metal ions often play an important role in RNA catalysis by activating a nucleophile for cleavage. Mg^{2+}, Mn^{2+}, and more rarely, Ca^{2+} and Zn^{2+}, have been shown to act as cofactors in metal-dependent RNases (Nowotny and Yang, 2006; Zhao et al., 2015). In some cases, individual RNases have been known to bind to a variety of divalent metal ions (Ando et al., 2021). Depending on the metal and the RNase, these metals can be inhibitory or activating. Because the metals in RNases are sometimes present for catalytic purposes over structural or RNA binding purposes, removing them can retain proper RNA binding, while disrupting RNase cleavage functions. Below we will give examples of methods used to remove or replace metals from active sites to assemble RNase–RNA complexes trapped in a state prior to RNA cleavage (Table 4; Fig. 7).

In cases of metal dependent catalysis, it is possible to inhibit cleavage simply by omitting metals from solutions used for protein extraction and purification. However, since metals can co-purify with RNases used for structural studies, the use of metal-chelating agents should be considered as well. Considerations for metal occupancy include dissociation constants and substrate dependence in the reaction scheme. The structure of *Aquifex aeolicus* RNase III bound to 46 mer dsRNA was solved by omitting metals to prevent cleavage (Table 4; Fig. 7A; (Gan et al., 2008). Positively charged metal ions are required for negatively charged RNA to bind productively to the negatively charged active site (Gan et al., 2008). Likely due to this, dsRNA in this *Aquifex aeolicus* RNase III–46 mer dsRNA structure was positioned outside of the active site (Fig. 7A), similar to when this enzyme was determined bound to 10 mer self-complementary dsRNA when it had a mutated active site residue designed to disrupt metal binding (Fig. 5B; Blaszczyk et al., 2004; Gan et al., 2008).

Ca^{2+} metal ions serve, in many cases, as inhibitory replacements within metal-dependent RNases (Rosta et al., 2014). Quantum and molecular mechanics free energy calculations were used by Rosta et al. (2014) to demonstrate that Ca^{2+} replacement of Mg^{2+} inhibits the prototypical RNase H1. The free energy barrier for the rate limiting step of the reaction is about 17 kcal/mol for when the active site contains Mg^{2+} contrasted with about 29 kcal/mol for Ca^{2+}; additionally, Ca^{2+} exhibits lower charge transfer efficacy than Mg^{2+} that contributes to a lack of assistance in activation of the nucleophile and as a result inhibits the catalytic reaction (Rosta et al., 2014). Calcium was present in the assembly buffer used to determine the cryo-electron microscopy (cryo-EM) structural models of *Homo sapiens* Dicer protein (hDicer; having two RNase III-like domains) bound to the transactivation response element RNA binding protein (TRBP) and 73 nucleotide (nt) pre-let-7 pre-miRNA. This inhibitory Ca^{2+} permitted trapping this complex pre-cleavage and therefore prior to let-7 product formation (Table 4; PDB: 5ZAL; (Liu et al., 2018). Two distinct conformational states or cryo-EM classes were identified, one pre- and, the other post-unwinding of the long dsRNA region of pre-let-7 that is thought to lead to generating single-stranded RNA sufficient to then reach an RNase III-like active site for cleavage. Ca^{2+} was not modeled into this structure, likely due to the limiting resolution of 4.7 Å.

Table 4
RNase–RNA structures solved using manipulated crystallization conditions.

RNase	PBD ID	Substrates	Method	Author
Aquifex aeolicus RNase III	2NUE	46 mer dsRNA	Metals omitted from crystallization conditions	(Gan et al., 2008)
Homo sapiens RNase III	5ZAL	Class I 73 mer pre-miRNA	Ca^{2+}	(Liu et al., 2018)
	5ZAM	Class II 73 mer pre-miRNA		
HIV type 1 RNase H	6BSH	23 mer DNA 25 mer RNA hybrid	Ca^{2+}	(Lan et al., 2018)
Thermotoga maritima RNase H	3O3G	12 mer dsDNA with single RNA 5′ to the scissile phosphate	Ca^{2+}	(Rychlik et al., 2010)
Alkalihalobacillus halodurans RNase H	2G8W	6 mer RNA/DNA hybrid	Ca^{2+}	(Nowotny and Yang, 2006)
Bacillus halodurans RNase H	6DMN	6 mer RNA/DNA hybrid	Ca^{2+}	(Samara and Yang, 2018)
Escherichia coli RNase T	3NH1	7 mer ssDNA	pH	(Hsiao et al., 2011)
	3V9X	7 mer ssDNA	pH	(Hsiao et al., 2012)
	3V9W	5 mer ssDNA	pH	
	3V9U	7 mer ssDNA	pH	
	4KB0	18 mer Bulge DNA (CC insertion)	pH	(Hsiao et al., 2014)
	4KB1	18 mer Bulge DNA (CT insertion)	pH	
Pyrococcus abyssi RNase PH ring	2PO1	10-mer poly (A)	Phosphate	(Navarro et al., 2008)

Ca^{2+} *was* modeled in the active site of the X-ray crystal structure of the inhibited HIV type 1 RNase H bound to a 25:23 mer DNA/RNA hybrid; to achieve this, Ca^{2+} was included in the crystallization solutions (Table 4; PDB: 6BSH; (Tian et al., 2018). In the structure of *Alkalihalobacillus halodurans* RNase H bound to a 6 mer RNA/DNA hybrid, the two Ca^{2+} ions in the active site maintained the typical 4 Å Mg^{2+}-Mg^{2+} distance and did not alter the RNase conformational state (Table 4; Fig. 7B; (Nowotny and Yang, 2006). In the structure of *Bacillus halodurans* RNase H bound to a 6 mer RNA/DNA hybrid, the two Ca^{2+} ions (Table 4; PDB: 6DMN; (Samara and Yang, 2018) are only 0.4 Å further from each other than the typical distance separating Mg^{2+} ions. In this latter study, Ca^{2+} was also used as a place holder during crystallization, followed by its removal with ethylene glycol-bis(β-aminoethyl ether)-N, N,N′,N′-tetraacetic acid (EGTA), a metal chelator, to then subsequently soak in different metal co-factors. After soaking, crystals were frozen at different time-points to structurally elucidate reaction coordinate intermediates. Interestingly, this *in crystallo* study revealed important roles of K^{+} ions, as well as identified a transient Mg^{2+} ion presence during the reaction mechanism, (Samara and Yang, 2018). The structure of *Thermotoga maritima* RNase H bound to 12 mer dsDNA with a single ribonucleotide 5′ to the scissile phosphate showed yet again that Ca^{2+}

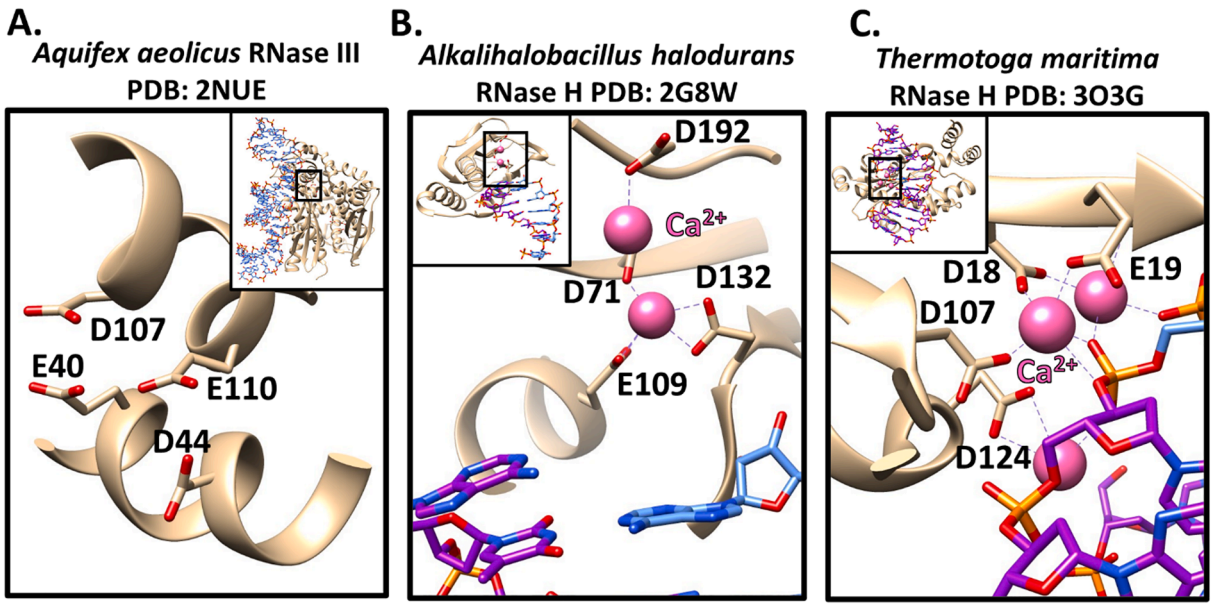

Fig. 7. X-Ray crystal structures of RNase–pre-cleavage substrate and/or substrate-mimic complexes that utilize metal ion chelation or replacement methods for inhibition. A.) 3.09 Å resolution X-ray crystal structure of *Aquifex aeolicus* RNase III bound to RNA. B.) 2.05 Å resolution X-ray crystal structure of *Alkalihalobacillus halodurans* RNase H bound to an RNA/DNA hybrid and two Ca^{2+} ions. C.) 2.10 Å resolution X-ray crystal structure of *Thermotoga maritima* RNase H2 bound to DNA with RNA modification and three Ca^{2+}.

ions can occupy active site metal ion positions similar to those that facilitate RNA cleavage (Table 4; Fig. 7C; (Rychlik et al., 2010).

Due to the nature of crystallization screening, conditions are often happenstance leaving the researcher unable to specifically dictate all solution components. It should be noted though, that some common crystallization condition components such as citric acid (and/or its conjugate base, citrate), which is often used for buffering pH, have metal chelating properties. As an example, one fourth of Joint Center for Structural Genomics crystallization JCSG-plus™ screen (Molecular Dimensions; MD1-37) conditions contain some form of citrate. Citric acid is a common food preservative that functions by chelating metals required for enzymes that cause spoilage (Furia, 1973). As an example, in the pre-catalytic (i.e. prior to RNA polymerization in this instance) substrate complex I of N4 mini-virion RNA polymerase bound to 36-mer DNA containing promoter and template, no catalytic metals were present in the active site despite the presence of 10 mM $MgCl_2$, and this was attributed to citric acid (from 0.11 M dibasic ammonium citrate) in the crystallization condition having a higher affinity for Mg^{2+} than the aspartic acids that coordinate the metals required for RNA phosphodiester bond formation (Gleghorn et al., 2011).

Manipulation of crystallization pH

RNase catalytic activity can be inhibited by altering solution pH; this is especially true given deprotonation and protonation steps in a typical RNase reaction scheme (Fig. 1). Solutions permitting crystallization might also promote enzymatic inactivation and therefore enhance the ability to determine the structure of an RNase–RNA pre-cleavage complex. Crystallization solutions like this could be identified serendipitously through screening and structure determination, or possibly by experimentally altering the pH of a known crystallization condition. Since deprotonation (high pH) and protonation (low pH) of active site residues could inhibit RNase activity, this alleviates the need for amino acid mutations, and could therefore possibly present a more accurate structural depiction of the wild-type enzyme. A caveat of course, at high pH, is the known un-enzymatic self-cleavage of RNA due to activation of a 2′–OH that is 5′ to the cut site, and also unwanted protein degradation.

The downfall in screening co-crystallization (i.e. RNase and RNA crystallized together) conditions only at pH values that inhibit RNase activity is that the optimal conditions for crystallization are often difficult to determine even without this restriction. Typically, crystallization conditions are very specific to a limited pH range, and can, for example, be associated with decreased protein solubility when near the protein isoelectric point (Zhang et al., 2013). However, the “gold standard” hen egg-white lysozyme protein produces similarly diffracting crystals grown at pH values from 2.5 to 6.5, or that are grown at pH 5.5 followed by soaking in a pH 8.0 solution (Iwai et al., 2008). Therefore, a likely potential remains for RNase researchers to find suitable inhibitory, yet crystallization promoting, and/or tolerating conditions to trap RNase–RNA pre-cleavage complexes for structure determination. In the opposite scenario, when identified co-crystallization conditions do permit RNase activity, RNA will like be cleaved resulting in a product complex structure; therefore, a possible strategy might be a crystal soaking procedure with a buffer pH that is inhibitory while simultaneously providing a new source of uncleaved RNA in the solution to replace prior cleaved products in the RNase active sites.

Finding conditions that grow crystals that also inhibit RNase activity is likely difficult and as such there are few examples. One example demonstrating this pH-controlling method, is that used to capture *E. coli* RNase T bound to DNA substrates. RNase T has a DEDDh active site, named for the residues involved and that coordinate two metals for catalysis (Table 4; Fig. 8; (Hsiao et al., 2011)). This RNase T is an exonuclease that trims 3′ ends, can be inhibited by a C base (the “C effect”) and double-stranded DNA, and can cleave RNA as well as DNA, actually binding DNA with a lower K_m than tRNA, for example (Hsiao et al., 2012; Hsiao et al., 2014; Hsiao et al., 2011; Viswanathan et al., 1998; Zuo and Deutscher, 1999; Zuo and Deutscher, 2002). Since this enzyme requires deprotonation of His181 to activate a water molecule for nucleophilic attack (that is coordinated by metal A), the pH 5.5–6.0 of crystallization conditions prevented this deprotonation and therefore water coordination and cleavage activity, albeit on DNA substrates in these cases (note that this is less consequential given the two-metal mechanism that does not directly require involvement of a 2′–OH from RNA (Hsiao et al., 2012; Hsiao et al., 2014; Hsiao et al., 2011). Six different X-ray crystal structures of RNase T bound to different DNA substrates have been determined using this method, elucidating the

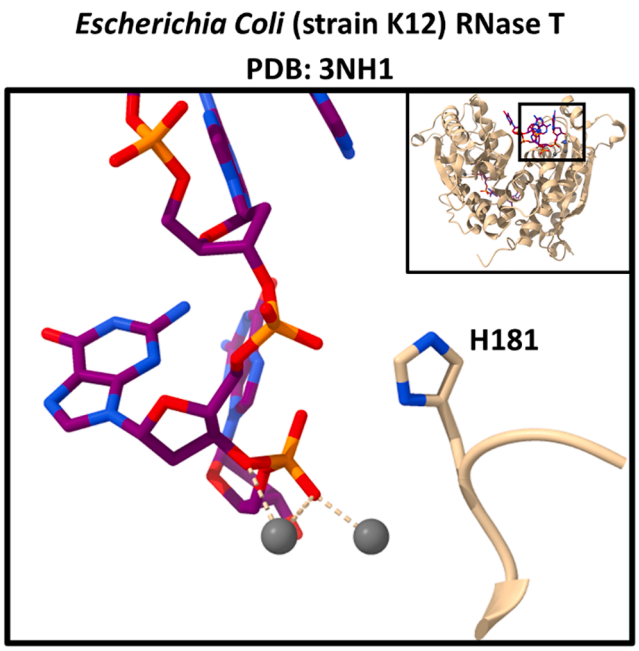

Fig. 8. An RNase–pre-cleavage substrate complex that was captured using pH inhibition. 2.11 Å X-ray crystal structure of *Escherichia coli* (strain K12) RNase T bound to ssDNA.

precise 3′ trimming activity and specificity of RNase T on different substrates (Hsiao et al., 2012; Hsiao et al., 2014; Hsiao et al., 2011). In Fig. 8 we show the determined structure of RNase T bound to ssDNA, as a representative example (Hsiao et al., 2011).

Manipulation of phosphate concentration

While not a universal strategy for all RNases described above, polynucleotide phosphorylases (PNPases) are a class of RNases that utilize phosphate to attack the scissile phosphate rather than water and produce a nucleoside diphosphate product through this S_N2 mechanism (Fig. 1C)(Briani et al., 2016; Navarro et al., 2008; Yang, 2011). These enzymes are actually performing the reverse reaction to a polymerase, albeit one using NDPs not NTPs as substrate, and can as such perform these functions presumably when the substrate and product balance is altered (Briani et al., 2016). Navarro et al. (Navarro et al., 2008) were able to capture the X-ray crystal structure of *Pyrococcus abyssi* exosome RNase PH core ring, formed by three Rrp41/Rrp42 heterodimers visualized after imposing a view of crystallographic symmetry mates, and bound to three, 10 mer uncleaved ssRNAs positioned at the active site(s) (Table 4; Fig. 9). While phosphate from phosphate buffered saline (PBS) was part of the protein solution, the authors describe that the lack of phosphate in the crystallization solution prevented ssRNA cleavage due to a lack of phosphate. Since 10 mer ssRNA was soaked into the crystal, rather than co-crystallized, we surmise that residual phosphate was more likely removed through this latter process. It should be noted that crystallographers often avoid phosphate in crystallization screens and protein solutions due to the appearance of false positive salt crystals especially with conditions containing positively charged metal ions; for PNPases the inclusion of phosphate in solutions appears to be a second important concern in this regard. A different interpretation is that lack of activating metals prevented RNA cleavage in their substrate-bound structure; authors used 5 mM $MgCl_2$ in their biochemical cleavage assays, however no Mg^{2+} was present in the crystallization or soaking experiments.

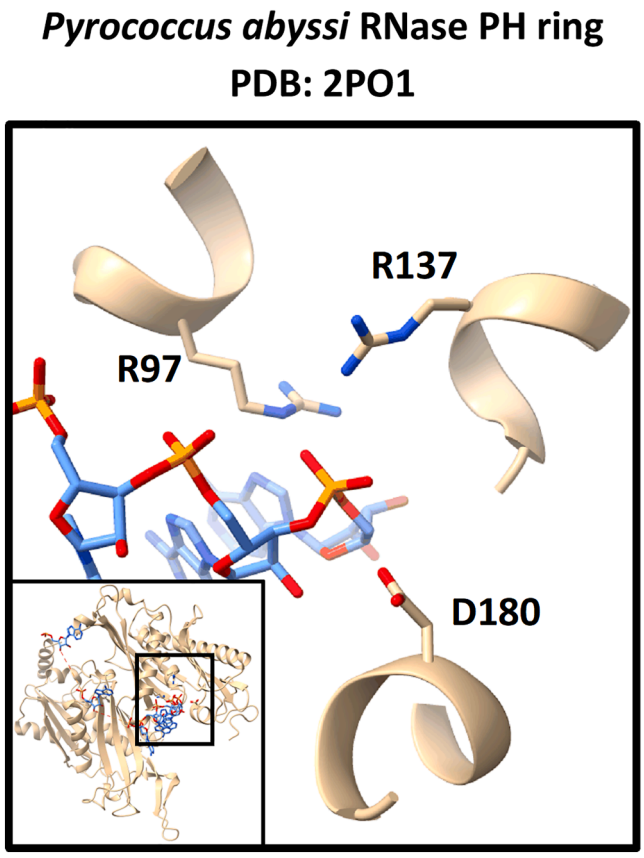

Fig. 9. An example of using phosphate depletion for inhibition to capture an RNase–pre-cleavage substrate complex. 1.94 Å resolution X-ray crystal structure of *Pyrococcus abyssi* RNase PH ring bound to three, 10 mer poly(rA) ssRNA strands. Only one Rrp41/Rrp42 heterodimer (of three) are shown for a clear view of RNA bound to the RNase.

RNase inhibitors

Ideally researchers could control RNase function by simply "switching off" cleavage activity while retaining pre-cleavage RNA binding. This concept in biochemistry is most closely related to "noncompetitive allosteric inhibition." In a publication regarding DEDDh nucleases RNase T and CRN-4, RNase inhibitors from the literature were nicely characterized as to whether nuclease activity or RNA binding were inhibited in their presence (Huang et al., 2016). If cleavage activity is inhibited but binding is not, then this suggests the potential for noncompetitive inhibition and therefore trapping an RNase–RNA pre-cleavage complex. Huang et al. determined the X-ray crystal structure of a cell death-related nuclease 4 (CRN-4) enzyme bound to MES (Table 5; Fig. 10A), an often used pH buffering molecule, and found the molecule bound in the active site where binding displaced an important

Table 5
RNase–RNase inhibitor structures that have been determined.

RNase	PBD ID	Inhibitor	Author
Caenorhabditis elegans CRN-4	5DK5	MES	(Huang et al., 2016)
Influenza A virus (A/California/04/2009 (H1N1)) PA endonuclease	5VPT	RO-7	(Jones et al., 2018)
Shigella flexneri VapC	5ECD	HEPES	(Xu et al., 2016)
Bos taurus RNase A	1RCA	Deoxycytidylyl-3′,5′-guanosine dinucleotide	(Listgarten et al., 1995)

histidine residue needed for catalysis (Huang et al., 2016). One metal ion is also bound in this structure and the authors pointed out in regards to a related work, it is likely the sulfuric group on MES that mimics a normal RNA phosphate group to support this binding (Huang et al., 2016). While no ssDNA was in this structure, the authors showed in biochemical experiments that RNA binding was retained in solution in the presence of MES, and other inhibitors. The authors then generated a theoretical CRN-4–RNA homology model and superimposed this onto their CRN-4–MES structure to show potential for simultaneous RNA and MES binding in the active site; future structures of RNase–RNA–inhibitor complexes, if achievable, could be of great value in this field of study. Another potential for trapping RNase–RNA pre-cleavage complexes is in aminoglycosides that have been shown to be noncompetitive inhibitors (in regards to RNA binding) to RNase P on pre-tRNA substrates, yet compete with Mg^{2+} binding (Tekos et al., 2000). In all cases however, a clear inhibitory molecule that also binds completely outside the RNA binding channel is elusive, yet nonetheless, identification of such molecules could lead to an improved ability to capture RNase–RNA pre-cleavage complexes.

Structures of RNases bound to competitive inhibitors in the absence of RNA substrate remain valuable especially in lieu of not having an existing RNase–RNA complex structure. Such models can provide the basis for subsequent computational modeling of RNA molecules into RNase active sites. This modeling can then be guided by interactions of the RNase and ligand molecule, especially those regions of the ligand that are similar to RNA components. For example, while competitive inhibitors typically bind the RNase active site and thereby do not permit cognate RNA binding, catalytic metals might be retained when bound to ligand in the active site as described below. A number of drugs bound in the active site of the endonuclease domain of the influenza virus RNA polymerase complex have been determined (Jones et al., 2018; Omoto et al., 2018; Song et al., 2016). These structures, coupled with mutagenesis experiments have worked towards understanding the binding landscape for future drug development coupled with site-directed mutagenesis to understand and predict mutant viral proteins that could evade such drugs. Interestingly, some of these molecules, such as RO-7, bind in the same active site as natural RNA substrate, while also coordinating two catalytic metals, mimicking the natural binding state for catalysis (Table 5; Fig. 10B). In the case of the bacterial tRNA nuclease VapC, a structure from *Shigella flexneri VapC* had a bound HEPES molecule in the active site (Table 5; Fig. 10C; (Xu et al., 2016). As there currently is no structure of a VapC protein bound to tRNA, accidental findings such as this, where a molecule somewhat shares attributes to the natural substrate, can be used to help build models and

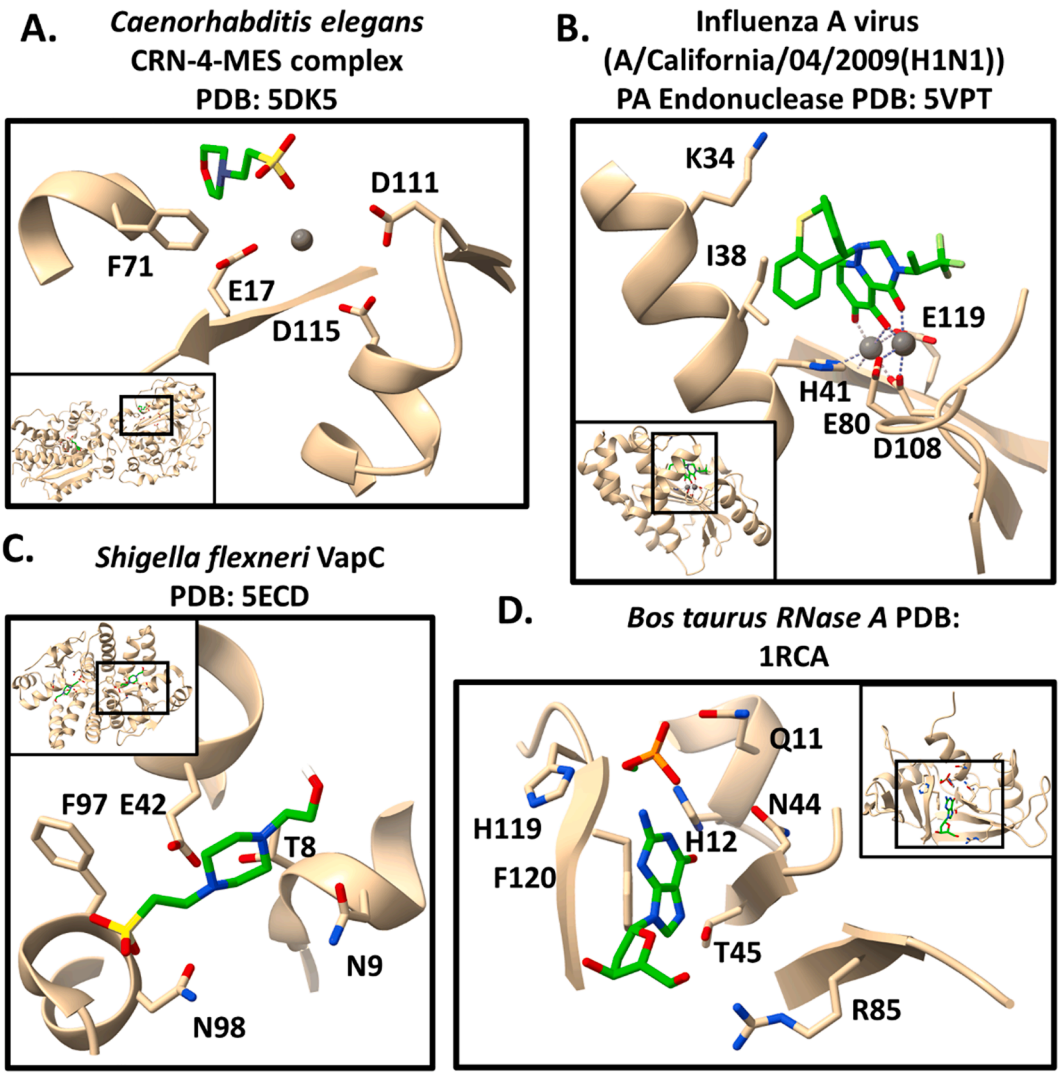

Fig. 10. RNases bound to RNase inhibitors A.) 2.10 Å resolution X-ray crystal structure of *Caenorhabditis elegans* CRN-4 bound to MES. B.) 2.10 Å resolution X-ray crystal structure of 2009 H1N1 PA endonuclease in complex with RO-7. C.) 1.75 Å resolution X-ray crystal structure of *Shigella flexneri* VapC bound to HEPES. D.) 1.90 Å resolution X-ray crystal structure of *Bos taurus* RNase A bound to deoxycytidylyl-3′,5′-guanosine dinucleotide.

educate future experiments towards capturing a true VapC–tRNA complex structure.

The intermediate stepping stone from structures of RNases bound to inhibitor molecules that mimic natural RNA substrates versus natural substrates pre-cleavage, is of RNases bound to inhibitors that have some nucleic acid composition. An example of this is a "retrobinding" inhibitor bound within a *Bos taurus* RNase A. In this case a threonine (T45) of the active site used to recognize pyrimidines does not recognize the purine guanosine base of a deoxycytidylyl-3′,5′-guanosine dinucleotide. This results in substrate binding in such a way to prevent scissile phosphate cleavage (Table 5; Fig. 10D; (Listgarten et al., 1995). In this instance, selectivity of this RNase is permitted while also capturing RNA in the active site.

Temperature snapshots

Enzymatic catalysis *in crystallo*, meaning occurring within a macromolecular crystal, is well documented (Geremia et al., 2002; Stewart et al., 2021). The major advantage of *in crystallo* catalysis is twofold, firstly it proves that crystal structures can be trusted to show the active conformation of an enzyme. Secondly, it makes it possible to collect structural data from catalytic reaction intermediates (Stoddard, 2001). Samara et. al. has taken advantage of *in crystallo* catalysis to develop a general freeze trapping method for DNA polymerase η, RNase H1, and endonuclease V (Samara et al., 2017). As a side note, when crystals are frozen at different time points, cryoprotectants that support quality diffraction such as polyethylene glycol or glycerol are used and will have to be optimized as part of this process. As one example of this freeze trapping method, Samara et. al. first co-crystalized RNase H1 and RNA substrate in buffer containing Ca^{2+} to prevent catalysis. Then, once crystals were fully matured, they were submerged in EGTA to remove Ca^{2+} so that it could be replaced temporarily by different monovalent metals. This step is important as Ca^{2+} is not readily outcompeted during soaking with Mg^{2+} or Mn^{2+} ions, as it is with monovalent ions. The next step, soaking the crystals in a Mg^{2+}/Mn^{2+} reaction buffer, activated the enzyme to start the reaction. The crystals were then soaked in the reaction buffer for different times prior to being frozen in liquid nitrogen to stop the reaction in its place (Samara et al., 2017). Using the above method, a crystal structure of WT RNase H1 in complex with bound uncleaved RNA/DNA substrate as well as two Mg^{2+} in the active site was solved (Table 6; Fig. 11A; PDB 6DMV; (Samara and Yang, 2018). The crystal was soaked in buffer containing 2 mM Mg^{2+} and 200 mM K^{+} for 40 s and frozen in liquid nitrogen. Though the necessary metals were properly placed in the active site, the nucleophilic water (shown in Fig. 11A) needed for the reaction was 3.3 Å and 20° away from its catalytic position as a result of the freeze trapping, causing the reaction to not take place.

The structure of *Mus musculus* endonuclease V in complex with substrate RNA with a deoxyinosine site (RNA(dI)) as well as the product and intermediate steps of the reaction was determined using the endonuclease V freeze trapping method (Samara et al., 2017; Wu et al., 2019). Co-crystals of endonuclease V and RNA(dI) were grown in the presence of Ca^{2+} to prevent cleavage. These crystals were then incubated in buffer containing 10 mM Mn^{2+} for varying amounts of time before being flash frozen to stop the reaction. After 2 min of soaking (Table 6; Fig. 11B; PDB: 6OZL; (Wu et al., 2019) there was no cleavage observed resulting in a pre-cleavage substrate structure. 100% cleavage was observed at the 180-minute mark (Table 6; Fig. 11C; PDB 6OZP; (Wu et al., 2019) and this crystal structure represents the post cleavage product state.

Table 6
RNase–RNA structures solved using temperature snapshots.

RNase	PBD ID	Substrate	Freezing Technique	Author
Bacillus halodurans RNase H1	6DMV	6 mer RNA/DNA hybrid	40 s soak in 2 mM Mg^{2+} followed by cryogenic freezing	(Samara and Yang, 2018)
Mus musculus endonuclease V	6OZL	23 mer RNA with a deoxyinosine	2 min soak in 10 mM Mn^{2+} followed by cryogenic freezing	(Wu et al., 2019)
	6OZP		180 min soak in 10 mM Mn^{2+} followed by cryogenic freezing	

Future ideas and considerations

Above, we have listed numerous successful techniques that have been used to trap a variety of RNase–RNA pre-cleavage complexes for structural determinations. The future of related work will involve the numerous RNase proteins yet undiscovered in nature, as well as the currently known RNases with currently unknown RNA substrate specificity. Here we list concepts that could be useful to future studies:

Existing product state complex crystal structures could be used as a starting place for solving RNase–RNA pre-cleavage complex crystal structures. Potentially, known (from the Protein Data Bank) conditions to produce RNase crystals bound to cleaved product can be regrown, and used as starting material for soaking experiments (Hassell et al., 2007). Product can then be exchanged with uncleavable modified RNA or with natural RNA that is cleavage-inhibited by environmental conditions, such as alteration of metal ion presence or composition, pH, or temperature. X-ray free-electron lasers might likely be used to rapidly collect X-ray crystal diffractions data, even at room temperature, versus the traditional cold temperatures of cryo-crystallography, to capture RNase–RNA pre-cleavage complexes directly after soaking natural substrates into the crystal (Schulz et al., 2018). This technique was used to determine the structure of fluoroacetate dehalogenase bound to substrate prior to cleavage as well as structures of this protein in different catalytic intermediate states. To achieve this, photo-activation of caged molecules in crystal pores permitted timed release of substrate (Mehrabi et al., 2019). The development for similar strategies to release cognate RNA molecules could be generated as a future strategy to determine RNase–RNA pre-cleavage complexes and even respective RNase-containing structures in subsequent catalytic intermediate states.

The development of chemical modifiers of RNase active site residues and nucleic acids will expand our capabilities to assemble RNase–RNA complexes. The future will provide new ways to modify WT active site amino acid R-groups chemically and new modifications in nucleic acids that render them similar in structure to their native form yet differ in composition. Of course, this will involve nucleic acid chemical synthesis expertise. For example, "XNA's" which are synthetic unnatural DNA or RNA molecules, could potentially be uncleavable and useful for substrate complex capturing (Nie et al., 2020). The role of biochemists will be to continue to validate and test these new modifications for their ability to affect cleavage of these mimic substrates. A variety of techniques can be used to test the interactions of RNases and nucleic acids that permit interaction without cleavage. Examples include DNA nanoswitches (Chandrasekaran et al., 2020) as well as in-cell techniques similar to yeast to hybrid analysis (Yang et al., 2018), and high throughput methods that have been used to identify interactions of RNA binding proteins and RNA (Cook et al., 2015).

Unmodified RNases and RNA substrates could be used in future cryo-EM studies. An impactful advantage of cryo-EM derives from freezing complexes in time and space, while eliminating the necessity of the crystallization step of X-ray crystallography. RNase inhibition methods presented in this review provide a clear bottleneck to RNase catalysis that can be used to assemble populations of the desired RNase–RNA complexes, as evidenced by Oreum et al. (Oerum et al., 2020) discussed above. The proven ability to observe transient reaction intermediates with cryo-EM (Dandey et al., 2020) also suggests the potential to use WT RNases and unmodified substrates in the future as well. Possibly, the use

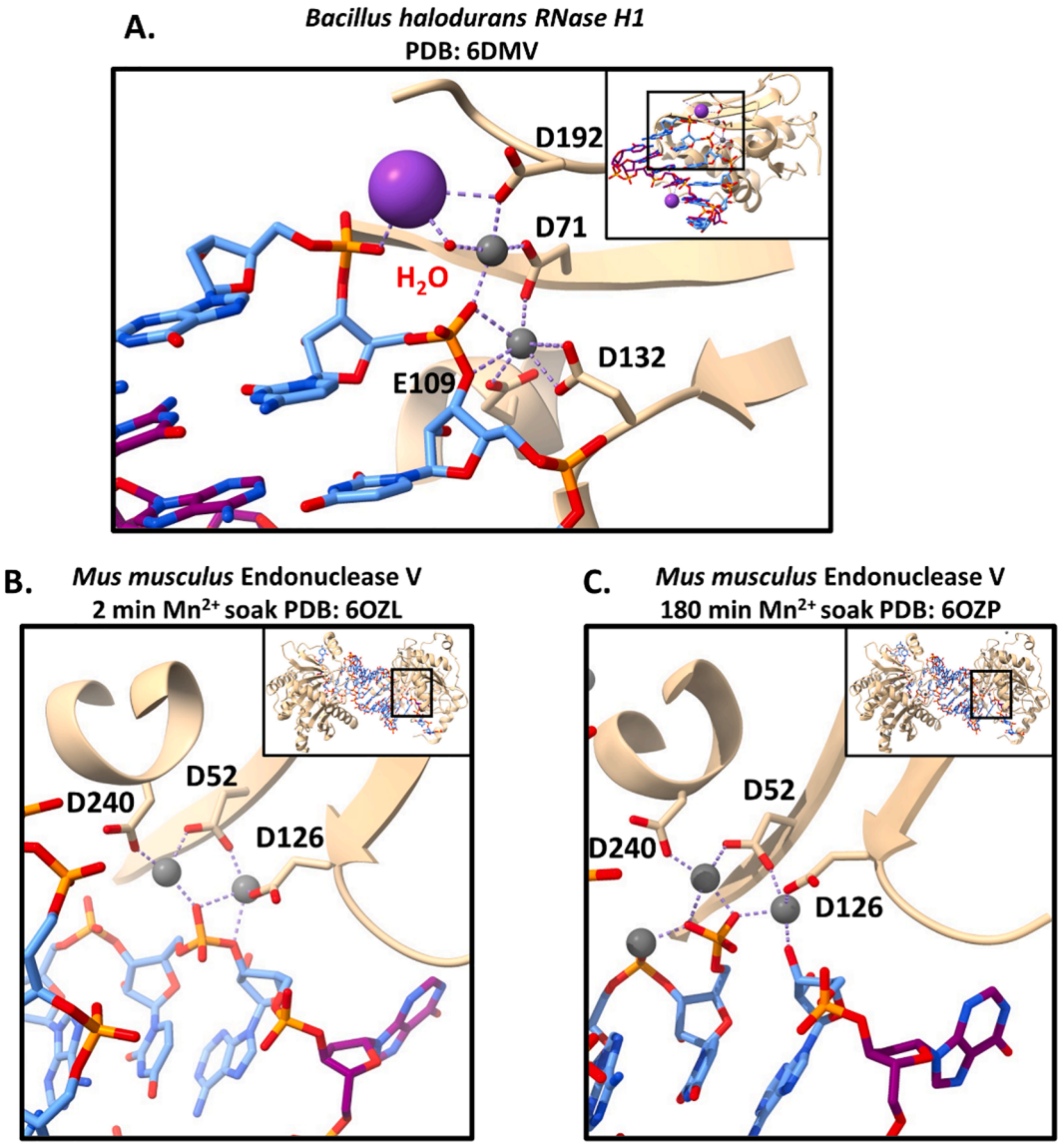

Fig. 11. RNase–pre-cleavage substrate complexes (A and B) and post cleavage product complexes (C) that use freeze trapping. Large purple spheres are K^+ ions, small red spheres are H_2O molecules. A.) 2.10 Å resolution X-ray crystal structure of an Endonuclease V bound to 23 mer RNA with a deoxyinosine after a 2 min Mn^{2+} soak. B.) 1.96 Å resolution X-ray crystal structure of an Endonuclease V bound to cleaved 23 mer RNA with a deoxyinosine after a 180 min Mn^{2+} soak. C.) 1.52 Å resolution X-ray crystal structure of RNase H1 bound to 6 mer RNA/DNA hybrid after a 40 s Mg^{2+} soak. (For interpretation of the references to colour in this figure legend, the reader is referred to the web version of this article.)

of cross-linking agents used to trap RNase–RNA complexes in cells (Majumder and Palanisamy, 2021), could aid trapping similar complexes in cryo-EM studies.

Deep learning by artificial intelligence will require more, and more diverse, experimental data to accurately predict RNase–RNA complexes in the future. An unprecedented ability to predict protein structures using deep learning by artificial intelligence (AI) has recently been achieved by AlphaFold2 (Jumper et al., 2021). A future goal should be to predict, to a similar level of accuracy, structures of RNase–RNA substrate complexes. AI has recently been used to improve RNA structure determination (Townshend et al., 2021). The future will likely combine AI prediction of both RNase and RNA structures separately, and later combined as RNase–RNA complex structures. A limitation to this goal is that structure datasets should include a diverse set of existing RNase–RNA complex structures important to "teach" these deep learning algorithms (Yang et al., 2020). Continued contribution to such datasets in the meantime using methods discussed in this review are important to this endeavor.

Funding

This work was supported by the RIT College of Science Emerson Summer Undergraduate Research Fellowship awarded to Seth Jones and Christian Goossen, the Dr. Terry Morrill Endowed Student Research Fund awarded to Sean Lewis and Seth Jones, and by the RIT College of Science Dean's Research Initiative Grant awarded to Dr. Michael Gleghorn.

Declaration of Competing Interest

The authors declare that they have no known competing financial interests or personal relationships that could have appeared to influence the work reported in this paper.

References

Abdur, R., Gerlits, O.O., Gan, J., Jiang, J., Salon, J., Kovalevsky, A.Y., Chumanevich, A. A., Weber, I.T., Huang, Z., 2014. Novel complex MAD phasing and RNase H structural insights using selenium oligonucleotides. Acta Crystallogr. D Biol. Crystallogr. 70, 354–361.

Abula, A., Li, X., Quan, X., Yang, T., Liu, Y., Guo, H., Li, T., Ji, X., 2021. Molecular mechanism of RNase R substrate sensitivity for RNA ribose methylation. Nucleic Acids Res. 49, 4738–4749.

Ahola, V., Aittokallio, T., Uusipaikka, E., Vihinen, M., 2004. Statistical methods for identifying conserved residues in multiple sequence alignment. Stat. Appl. Genet. Mol. Biol. 3, Article28.

Aman, R., Ali, Z., Butt, H., Mahas, A., Aljedaani, F., Khan, M.Z., Ding, S., Mahfouz, M., 2018. RNA virus interference via CRISPR/Cas13a system in plants. Genome Biol. 19, 1.

Amblar, M., Arraiano, C.M., 2005. A single mutation in Escherichia coli ribonuclease II inactivates the enzyme without affecting RNA binding. FEBS J. 272, 363–374.

Ando, T., Jongruja, N., Okumura, N., Morikawa, K., Kanaya, S., Takao, T., 2021. Identification of the ternary complex of ribonuclease HI:RNA/DNA hybrid:metal ions by ESI mass spectrometry. J. Biol. Chem. 296, 100462.

Antoniali, G., Serra, F., Lirussi, L., Tanaka, M., D'Ambrosio, C., Zhang, S., Radovic, S., Dalla, E., Ciani, Y., Scaloni, A., Li, M., Piazza, S., Tell, G., 2017. Mammalian APE1 controls miRNA processing and its interactome is linked to cancer RNA metabolism. Nat. Commun. 8, 797.

Arni, R.K., Watanabe, L., Ward, R.J., Kreitman, R.J., Kumar, K., Walz, F.G., 1999. Three-dimensional structure of ribonuclease T1 complexed with an isosteric phosphonate substrate analogue of GpU: alternate substrate binding modes and catalysis. Biochemistry 38, 2452–2461.

Baek, M., DiMaio, F., Anishchenko, I., Dauparas, J., Ovchinnikov, S., Lee, G.R., Wang, J., Cong, Q., Kinch, L.N., Schaeffer, R.D., Millán, C., Park, H., Adams, C., Glassman, C. R., DeGiovanni, A., Pereira, J.H., Rodrigues, A.V., van Dijk, A.A., Ebrecht, A.C., Opperman, D.J., Sagmeister, T., Buhlheller, C., Pavkov-Keller, T., Rathinaswamy, M. K., Dalwadi, U., Yip, C.K., Burke, J.E., Garcia, K.C., Grishin, N.V., Adams, P.D., Read, R.J., Baker, D., 2021. Accurate prediction of protein structures and interactions using a three-track neural network. Science 373 (6557), 871–876.

Bandyra, K.J., Wandzik, J.M., Luisi, B.F., 2018. Substrate recognition and autoinhibition in the central ribonuclease RNase E. Mol. Cell 72 (2), 275–285.e4.

Bechhofer, D.H., Deutscher, M.P., 2019. Bacterial ribonucleases and their roles in RNA metabolism. Crit. Rev. Biochem. Mol. Biol. 54 (3), 242–300.

Becknell, B., Eichler, T.E., Beceiro, S., Li, B., Easterling, R.S., Carpenter, A.R., James, C. L., McHugh, K.M., Hains, D.S., Partida-Sanchez, S., Spencer, J.D., 2015. Ribonucleases 6 and 7 have antimicrobial function in the human and murine urinary tract. Kidney Int. 87 (1), 151–161.

Bhagwat, M., Meara, D., Nossal, N.G., 1997. Identification of residues of T4 RNase H required for catalysis and DNA binding. J. Biol. Chem. 272 (45), 28531–28538.

Blaszczyk, J., Gan, J., Tropea, J.E., Court, D.L., Waugh, D.S., Ji, X., 2004. Noncatalytic assembly of ribonuclease III with double-stranded RNA. Structure 12 (3), 457–466.

Briani, F., Carzaniga, T., Dehò, G., 2016. Regulation and functions of bacterial PNPase. Wiley Interdiscip Rev RNA 7 (2), 241–258.

Burmistrz, M., Krakowski, K., Krawczyk-Balska, A., 2020. RNA-targeting CRISPR-Cas systems and their applications. Int. J. Mol. Sci. 21 (3), 1122.

Callaghan, A.J., Marcaida, M.J., Stead, J.A., McDowall, K.J., Scott, W.G., Luisi, B.F., 2005. Structure of escherichia coli RNase E catalytic domain and implications for RNA turnover. Nature 437 (7062), 1187–1191.

Carte, J., Pfister, N.T., Compton, M.M., Terns, R.M., Terns, M.P., 2010. Binding and cleavage of CRISPR RNA by Cas6. RNA 16 (11), 2181–2188.

Carzaniga, T., Sbarufatti, G., Briani, F., Dehò, G., 2017. Polynucleotide phosphorylase is implicated in homologous recombination and DNA repair in Escherichia coli. BMC Microbiol. 17, 81.

Cerritelli, S.M., Crouch, R.J., 2009. Ribonuclease H: the enzymes in eukaryotes. FEBS J. 276, 1494–1505.

Chandrasekaran, A.R., Trivedi, R., Halvorsen, K., 2020. Ribonuclease-Responsive DNA Nanoswitches. Cell Rep. Phys. Sci. 1 (7), 100117.

Cook, K.B., Hughes, T.R., Morris, Q.D., 2015. High-throughput characterization of protein-RNA interactions. Brief Funct Genomics 14 (1), 74–89.

Court, D.L., Gan, J., Liang, Y.-H., Shaw, G.X., Tropea, J.E., Costantino, N., Waugh, D.S., Ji, X., 2013. RNase III: Genetics and function; structure and mechanism. Annu. Rev. Genet. 47 (1), 405–431.

Cuchillo, C.M., Nogués, M.V., Raines, R.T., 2011. Bovine pancreatic ribonuclease: fifty years of the first enzymatic reaction mechanism. Biochemistry 50 (37), 7835–7841.

Dandey, V.P., Budell, W.C., Wei, H., Bobe, D., Maruthi, K., Kopylov, M., Eng, E.T., Kahn, P.A., Hinshaw, J.E., Kundu, N., Nimigean, C.M., Fan, C., Sukomon, N., Darst, S.A., Saecker, R.M., Chen, J., Malone, B., Potter, C.S., Carragher, B., 2020. Time-resolved cryo-EM using Spotiton. Nat. Methods 17 (9), 897–900.

Devos, J.M., Tomanicek, S.J., Jones, C.E., Nossal, N.G., Mueser, T.C., 2007. Crystal structure of bacteriophage T4 5' nuclease in complex with a branched DNA reveals how flap endonuclease-1 family nucleases bind their substrates. J. Biol. Chem. 282 (43), 31713–31724.

Dorléans, A., Li de la Sierra-Gallay, I., Piton, J., Zig, L., Gilet, L., Putzer, H., Condon, C., 2011. Molecular basis for the recognition and cleavage of RNA by the bifunctional 5'-3' exo/endoribonuclease RNase. J. Structure 19 (9), 1252–1261.

El-Ashram, S., Al Nasr, I., Suo, X., 2016. Nucleic acid protocols: extraction and optimization. Biotechnol. Rep. (Amst) 12, 33–39.

Figiel, M., Nowotny, M., 2014. Crystal structure of RNase H3-substrate complex reveals parallel evolution of RNA/DNA hybrid recognition. Nucleic Acids Res. 42 (14), 9285–9294.

Frazão, C., McVey, C.E., Amblar, M., Barbas, A., Vonrhein, C., Arraiano, C.M., Carrondo, M.A., 2006. Unravelling the dynamics of RNA degradation by ribonuclease II and its RNA-bound complex. Nature 443 (7107), 110–114.

Freije, C.A., Myhrvold, C., Boehm, C.K., Lin, A.E., Welch, N.L., Carter, A., Metsky, H.C., Luo, C.Y., Abudayyeh, O.O., Gootenberg, J.S., Yozwiak, N.L., Zhang, F., Sabeti, P.C., 2019. Programmable inhibition and detection of RNA viruses using Cas13. Mol. Cell 76 (5), 826–837.e11.

Freudenthal, B.D., Beard, W.A., Cuneo, M.J., Dyrkheeva, N.S., Wilson, S.H., 2015. Capturing snapshots of APE1 processing DNA damage. Nat. Struct. Mol. Biol. 22 (11), 924–931.

Furia, T.E., 1973. CRC Handbook of Food Additives. Second Edition Taylor & Francis.

Gan, J., Tropea, J.E., Austin, B.P., Court, D.L., Waugh, D.S., Ji, X., 2005. Intermediate states of ribonuclease III in complex with double-stranded RNA. Structure 13 (10), 1435–1442.

Gan, J., Shaw, G., Tropea, J.E., Waugh, D.S., Court, D.L., Ji, X., 2008. A stepwise model for double-stranded RNA processing by ribonuclease III. Mol. Microbiol. 67, 143–154.

Geremia, S., Campagnolo, M., Schinzel, R., Johnson, L.N., 2002. Enzymatic catalysis in crystals of Escherichia coli maltodextrin phosphorylase. J. Mol. Biol. 322 (2), 413–423.

Gleghorn, M.L., Davydova, E.K., Basu, R., Rothman-Denes, L.B., Murakami, K.S., 2011. X-ray crystal structures elucidate the nucleotidyl transfer reaction of transcript initiation using two nucleotides. Proc. Natl. Acad. Sci. U.S.A. 108 (9), 3566–3571.

Golden, B.L., 2011. Two distinct catalytic strategies in the hepatitis delta virus ribozyme cleavage reaction. Biochemistry 50 (44), 9424–9433.

Gyi, J.I., Conn, G.L., Lane, A.N., Brown, T., 1996. Comparison of the thermodynamic stabilities and solution conformations of DNA·RNA hybrids containing purine-rich and pyrimidine-rich strands with DNA and RNA duplexes. Biochemistry 35 (38), 12538–12548.

Gyi, J.I., Lane, A.N., Conn, G.L., Brown, T., 1998. Solution structures of DNA.RNA hybrids with purine-rich and pyrimidine-rich strands: comparison with the homologous DNA and RNA duplexes. Biochemistry 37, 73–80.

Han, Y., Donovan, J., Rath, S., Whitney, G., Chitrakar, A., Korennykh, A., 2014. Structure of human RNase L reveals the basis for regulated RNA decay in the IFN response. Science 343 (6176), 1244–1248.

Haruki, M., Noguchi, E., Kanaya, S., Crouch, R.J., 1997. Kinetic and stoichiometric analysis for the binding of Escherichia coli ribonuclease HI to RNA-DNA hybrids using surface plasmon resonance. J. Biol. Chem. 272 (35), 22015–22022.

Hassell, A.M., An, G., Bledsoe, R.K., Bynum, J.M., Carter, H.L., Deng, S.-J., Gampe, R.T., Grisard, T.E., Madauss, K.P., Nolte, R.T., Rocque, W.J., Wang, L., Weaver, K.L., Williams, S.P., Wisely, G.B., Xu, R., Shewchuk, L.M., 2007. Crystallization of protein-ligand complexes. Acta Crystallogr. D Biol. Crystallogr. 63 (1), 72–79.

Healey, A., Furtado, A., Cooper, T., Henry, R.J., 2014. Protocol: a simple method for extracting next-generation sequencing quality genomic DNA from recalcitrant plant species. Plant Methods 10 (1), 21.

Henneke, M., Diekmann, S., Ohlenbusch, A., Kaiser, J., Engelbrecht, V., Kohlschütter, A., Krätzner, R., Madruga-Garrido, M., Mayer, M., Opitz, L., Rodriguez, D., Rüschendorf, F., Schumacher, J., Thiele, H., Thoms, S., Steinfeld, R., Nürnberg, P., Gärtner, J., 2009. RNASET2-deficient cystic leukoencephalopathy resembles congenital cytomegalovirus brain infection. Nat. Genet. 41 (7), 773–775.

Hou, T., Zeng, W., Yang, M., Chen, W., Ren, L., Ai, J., Wu, J., Liao, Y., Gou, X., Li, Y., Wang, X., Su, H., Gu, B., Wang, J., Xu, T., 2020. Development and Evaluation of A CRISPR-based Diagnostic For 2019-novel Coronavirus. medRxiv, 2020.2002.2022.20025460.

Howard, M.J., Lim, W.H., Fierke, C.A., Koutmos, M., 2012. Mitochondrial ribonuclease P structure provides insight into the evolution of catalytic strategies for precursor-tRNA 5' processing. Proc. Natl. Acad. Sci. U.S.A. 109 (40), 16149–16154.

Hsiao, Y.Y., Duh, Y., Chen, Y.P., Wang, Y.T., Yuan, H.S., 2012. How an exonuclease decides where to stop in trimming of nucleic acids: crystal structures of RNase T-product complexes. Nucleic Acids Res. 40, 8144–8154.

Hsiao, Y.-Y., Fang, W.-H., Lee, C.-C., Chen, Y.-P., Yuan, H.S., Petsko, G.A., 2014. Structural insights into DNA repair by RNase T–an exonuclease processing 3' end of structured DNA in repair pathways. PLoS Biol. 12 (3), e1001803.

Hsiao, Y.-Y., Yang, C.-C., Lin, C.L., Lin, J.L.J., Duh, Y., Yuan, H.S., 2011. Structural basis for RNA trimming by RNase T in stable RNA 3'-end maturation. Nat. Chem. Biol. 7 (4), 236–243.

Huang, K.-W., Hsu, K.-C., Chu, L.-Y., Yang, J.-M., Yuan, H.S., Hsiao, Y.-Y., 2016. Identification of inhibitors for the DEDDh family of exonucleases and a unique inhibition mechanism by crystal structure analysis of CRN-4 bound with 2-morpholin-4-ylethanesulfonate (MES). J. Med. Chem. 59 (17), 8019–8029.

Iqbal, M., Poole, E., Goodbourn, S., McCauley, J.W., 2004. Role for bovine viral diarrhea virus Erns glycoprotein in the control of activation of beta interferon by double-stranded RNA. J. Virol. 78 (1), 136–145.

Ishii, R., Nureki, O., Yokoyama, S., 2003. Crystal structure of the tRNA processing enzyme RNase PH from Aquifex aeolicus. J. Biol. Chem. 278 (34), 32397–32404.

Iwai, W., Yagi, D., Ishikawa, T., Ohnishi, Y., Tanaka, I., Niimura, N., 2008. Crystallization and evaluation of hen egg-white lysozyme crystals for protein pH titration in the crystalline state. J. Synchrotron Radiat. 15 (3), 312–315.

Jones, J.C., Kumar, G., Barman, S., Najera, I., White, S.W., Webby, R.J., Govorkova, E.A., Subbarao, K., 2018. Identification of the I38T PA Substitution as a Resistance Marker for Next-Generation Influenza Virus Endonuclease Inhibitors. mBio 9 (2).

Jumper, J., Evans, R., Pritzel, A., Green, T., Figurnov, M., Ronneberger, O., Tunyasuvunakool, K., Bates, R., Žídek, A., Potapenko, A., Bridgland, A., Meyer, C., Kohl, S.A.A., Ballard, A.J., Cowie, A., Romera-Paredes, B., Nikolov, S., Jain, R., Adler, J., Back, T., Petersen, S., Reiman, D., Clancy, E., Zielinski, M., Steinegger, M., Pacholska, M., Berghammer, T., Bodenstein, S., Silver, D., Vinyals, O., Senior, A.W.,

Kavukcuoglu, K., Kohli, P., Hassabis, D., 2021. Highly accurate protein structure prediction with AlphaFold. Nature 596 (7873), 583–589.
Junge, K., Eicken, H., Swanson, B.D., Deming, J.W., 2006. Bacterial incorporation of leucine into protein down to -20 degrees C with evidence for potential activity in sub-eutectic saline ice formations. Cryobiology 52, 417–429.
Kang, H., Hong, T., Lee, M., 2019. Technical performance analysis of the smart solar photovoltaic blinds based on the solar tracking methods considering the climate factors. Energy Build. 190, 34–48.
Kawai, G., Yamamoto, Y., Kamimura, T., Masegi, T., Sekine, M., Hata, T., Iimori, T., Watanabe, T., Miyazawa, T., Yokoyama, S., 1992. Conformational rigidity of specific pyrimidine residues in tRNA arises from posttranscriptional modifications that enhance steric interaction between the base and the 2'-hydroxyl group. Biochemistry 31 (4), 1040–1046.
Kellner, M.J., Koob, J.G., Gootenberg, J.S., Abudayyeh, O.O., Zhang, F., 2019. SHERLOCK: nucleic acid detection with CRISPR nucleases. Nat. Protoc. 14 (10), 2986–3012.
Kim, W.C., King, D., Lee, C.H., 2010. RNA-cleaving properties of human apurinic/apyrimidinic endonuclease 1 (APE1). Int. J. Biochem. Mol. Biol. 1, 12–25.
Kime, L., Jourdan, S.S., Stead, J.A., Hidalgo-Sastre, A., McDowall, K.J., 2010. Rapid cleavage of RNA by RNase E in the absence of 5' monophosphate stimulation. Mol. Microbiol. 76, 590–604.
Knott, G.J., East-Seletsky, A., Cofsky, J.C., Holton, J.M., Charles, E., O'Connell, M.R., Doudna, J.A., 2017. Guide-bound structures of an RNA-targeting A-cleaving CRISPR-Cas13a enzyme. Nat. Struct. Mol. Biol. 24, 825–833.
Koslover, D.J., Callaghan, A.J., Marcaida, M.J., Garman, E.F., Martick, M., Scott, W.G., Luisi, B.F., 2008. The crystal structure of the Escherichia coli RNase E apoprotein and a mechanism for RNA degradation. Structure 16, 1238–1244.
Krey, T., Bontems, F., Vonrhein, C., Vaney, M.C., Bricogne, G., Rümenapf, T., Rey, F.A., 2012. Crystal structure of the pestivirus envelope glycoprotein E(rns) and mechanistic analysis of its ribonuclease activity. Structure 20, 862–873.
Kumar, G., Cuypers, M., Webby, R.R., Webb, T.R., White, S.W., 2021. Structural insights into the substrate specificity of the endonuclease activity of the influenza virus cap-snatching mechanism. Nucleic Acids Res. 49, 1609–1618.
Lan, P., Tan, M., Zhang, Y., Niu, S., Chen, J., Shi, S., Qiu, S., Wang, X., Peng, X., Cai, G., Cheng, H., Wu, J., Li, G., Lei, M., 2018. Structural insight into precursor tRNA processing by yeast ribonuclease P. Science 362.
Lapkouski, M., Tian, L., Miller, J.T., Le Grice, S.F.J., Yang, W., 2013. Complexes of HIV-1 RT, NNRTI and RNA/DNA hybrid reveal a structure compatible with RNA degradation. Nat. Struct. Mol. Biol. 20, 230–236.
Lee, C.W., Park, S.H., Jeong, C.S., Cha, S.S., Park, H., Lee, J.H., 2019. Structural basis of small RNA hydrolysis by oligoribonuclease (CpsORN) from Colwellia psychrerythraea strain 34H. Sci. Rep. 9, 2649.
Leu, Y.J., Chern, S.S., Wang, S.C., Hsiao, Y.Y., Amiraslanov, I., Liaw, Y.C., Liao, Y.D., 2003. Residues involved in the catalysis, base specificity, and cytotoxicity of ribonuclease from Rana catesbeiana based upon mutagenesis and X-ray crystallography. J. Biol. Chem. 278, 7300–7309.
Lewis, K., 2007. Persister cells, dormancy and infectious disease. Nat. Rev. Microbiol. 5, 48–56.
Li de la Sierra-Gallay, I., Pellegrini, O., Condon, C., 2005. Structural basis for substrate binding, cleavage and allostery in the tRNA maturase RNase Z. Nature 433, 657–661.
Li de la Sierra-Gallay, I., Mathy, N., Pellegrini, O., Condon, C., 2006. Structure of the ubiquitous 3' processing enzyme RNase Z bound to transfer RNA. Nat. Struct. Mol. Biol. 13, 376–377.
Listgarten, J.N., Maes, D., Wyns, L., Aguilar, C.F., Palmer, R.A., 1995. Structure of the crystalline complex of deoxycytidylyl-3',5'-guanosine (3',5'-dCpdG) cocrystallized with ribonuclease at 1.9 A resolution. Acta Crystallogr. D Biol. Crystallogr. 51, 767–771.
Liu, L., Li, X., Ma, J., Li, Z., You, L., Wang, J., Wang, M., Zhang, X., Wang, Y., 2017. The Molecular Architecture for RNA-Guided RNA Cleavage by Cas13a. Cell 170, 714–726.e710.
Liu, Z., Wang, J., Cheng, H., Ke, X., Sun, L., Zhang, Q.C., Wang, H.W., 2018. Cryo-EM structure of human dicer and its complexes with a pre-miRNA substrate. Cell 173, 1191–1203.e1112.
Lorentzen, E., Basquin, J., Tomecki, R., Dziembowski, A., Conti, E., 2008. Structure of the active subunit of the yeast exosome core, Rrp44: diverse modes of substrate recruitment in the RNase II nuclease family. Mol. Cell 29, 717–728.
Loverix, S., Winqvist, A., Strömberg, R., Steyaert, J., 2000. Mechanism of RNase T1: concerted triester-like phosphoryl transfer via a catalytic three-centered hydrogen bond. Chem. Biol. 7, 651–658.
Luhtala, N., Parker, R., 2010. T2 Family ribonucleases: ancient enzymes with diverse roles. Trends Biochem. Sci. 35, 253–259.
Mackie, G.A., 1998. Ribonuclease E is a 5'-end-dependent endonuclease. Nature 395, 720–723.
Majumder, M., Palanisamy, V., 2021. Compendium of Methods to Uncover RNA-Protein Interactions In Vivo. Methods Protoc 4.
Malek-Adamian, E., Patrascu, M.B., Jana, S.K., Martínez-Montero, S., Moitessier, N., Damha, M.J., 2018. Adjusting the structure of 2'-modified nucleosides and oligonucleotides via C4'-α-F or C4'-α-OMe substitution: synthesis and conformational analysis. J. Org. Chem. 83, 9839–9849.
Matos, R.G., Bárria, C., Moreira, R.N., Barahona, S., Domingues, S., Arraiano, C.M., 2014. The importance of proteins of the RNase II/RNB-family in pathogenic bacteria. Front. Cell. Infect. Microbiol. 4, 68.
Mehrabi, P., Schulz, E.C., Dsouza, R., Müller-Werkmeister, H.M., Tellkamp, F., Miller, R. J.D., Pai, E.F., 2019. Time-resolved crystallography reveals allosteric communication aligned with molecular breathing. Science 365, 1167–1170.
Mignon, P., Steyaert, J., Loris, R., Geerlings, P., Loverix, S., 2002. A nucleophile activation dyad in ribonucleases. A combined X-ray crystallographic/ab initio quantum chemical study. J. Biol. Chem. 277, 36770–36774.
Navarro, M.V., Oliveira, C.C., Zanchin, N.I., Guimarães, B.G., 2008. Insights into the mechanism of progressive RNA degradation by the archaeal exosome. J. Biol. Chem. 283, 14120–14131.
Nelles, D.A., Fang, M.Y., O'Connell, M.R., Xu, J.L., Markmiller, S.J., Doudna, J.A., Yeo, G.W., 2016. Programmable RNA Tracking in Live Cells with CRISPR/Cas9. Cell 165, 488–496.
Nie, P., Bai, Y., Mei, H., 2020. Synthetic life with alternative nucleic acids as genetic materials. Molecules 25.
Niewoehner, O., Jinek, M., Doudna, J.A., 2014. Evolution of CRISPR RNA recognition and processing by Cas6 endonucleases. Nucleic Acids Res. 42, 1341–1353.
Nilsen, T.W., 2014. RNase footprinting to map sites of RNA-protein interactions. Cold Spring Harb Protoc 2014, 677–682.
Nowotny, M., Yang, W., 2006. Stepwise analyses of metal ions in RNase H catalysis from substrate destabilization to product release. EMBO J. 25, 1924–1933.
Nowotny, M., Gaidamakov, S.A., Crouch, R.J., Yang, W., 2005. Crystal structures of RNase H bound to an RNA/DNA hybrid: substrate specificity and metal-dependent catalysis. Cell 121, 1005–1016.
Nowotny, M., Gaidamakov, S.A., Ghirlando, R., Cerritelli, S.M., Crouch, R.J., Yang, W., 2007. Structure of human RNase H1 complexed with an RNA/DNA hybrid: insight into HIV reverse transcription. Mol. Cell 28, 264–276.
Oerum, S., Dendooven, T., Catala, M., Gilet, L., Dégut, C., Trinquier, A., Bourguet, M., Barraud, P., Cianferani, S., Luisi, B.F., Condon, C., Tisné, C., 2020. Structures of B. subtilis maturation rnases captured on 50S Ribosome with Pre-rRNAs. Mol. Cell 80, 227–236.e225.
Omoto, S., Speranzini, V., Hashimoto, T., Noshi, T., Yamaguchi, H., Kawai, M., Kawaguchi, K., Uehara, T., Shishido, T., Naito, A., Cusack, S., 2018. Characterization of influenza virus variants induced by treatment with the endonuclease inhibitor baloxavir marboxil. Sci. Rep. 8, 9633.
Pallan, P.S., Egli, M., 2008. Insights into RNA/DNA hybrid recognition and processing by RNase H from the crystal structure of a non-specific enzyme-dsDNA complex. Cell Cycle 7, 2562–2569.
Pallan, P.S., Prakash, T.P., de Leon, A.R., Egli, M., 2016. Limits of RNA 2'-OH mimicry by fluorine: crystal structure of bacillus halodurans RNase H bound to a 2'-FRNA:Dna Hybrid. Biochemistry 55, 5321–5325.
Pellegrini, O., Li de la Sierra-Gallay, I., Piton, J., Gilet, L., Condon, C., 2012. Activation of tRNA maturation by downstream uracil residues in B. subtilis. Structure 20, 1769–1777.
Pettersen, E.F., Goddard, T.D., Huang, C.C., Couch, G.S., Greenblatt, D.M., Meng, E.C., Ferrin, T.E., 2004. UCSF Chimera–a visualization system for exploratory research and analysis. J. Comput. Chem. 25, 1605–1612.
Rodriguez, S.M., Panjikar, S., Van Belle, K., Wyns, L., Messens, J., Loris, R., 2008. Nonspecific base recognition mediated by water bridges and hydrophobic stacking in ribonuclease I from Escherichia coli. Protein Sci. 17, 681–690.
Rosta, E., Yang, W., Hummer, G., 2014. Calcium inhibition of ribonuclease H1 two-metal ion catalysis. J. Am. Chem. Soc. 136, 3137–3144.
Rychlik, M.P., Chon, H., Cerritelli, S.M., Klimek, P., Crouch, R.J., Nowotny, M., 2010. Crystal structures of RNase H2 in complex with nucleic acid reveal the mechanism of RNA-DNA junction recognition and cleavage. Mol. Cell 40, 658–670.
Samara, N.L., Yang, W., 2018. Cation trafficking propels RNA hydrolysis. Nat. Struct. Mol. Biol. 25, 715–721.
Samara, N.L., Gao, Y., Wu, J., Yang, W., 2017. Detection of Reaction Intermediates in Mg^{2+}-dependent DNA synthesis and RNA degradation by time-resolved X-ray crystallography. Methods Enzymol. 592, 283–327.
Sarafianos, S.G., Marchand, B., Das, K., Himmel, D.M., Parniak, M.A., Hughes, S.H., Arnold, E., 2009. Structure and function of HIV-1 reverse transcriptase: molecular mechanisms of polymerization and inhibition. J. Mol. Biol. 385, 693–713.
Schneider, R., Unger, G., Stark, R., Schneider-Scherzer, E., Thiel, H.J., 1993. Identification of a structural glycoprotein of an RNA virus as a ribonuclease. Science 261, 1169–1171.
Schultz, L.W., Quirk, D.J., Raines, R.T., 1998. His...Asp catalytic dyad of ribonuclease A: structure and function of the wild-type, D121N, and D121A enzymes. Biochemistry 37, 8886–8898.
Schultz, S.J., Champoux, J.J., 2008. RNase H activity: structure, specificity, and function in reverse transcription. Virus Res. 134, 86–103.
Schultz, S.J., Zhang, M., Champoux, J.J., 2010. Multiple nucleotide preferences determine cleavage-site recognition by the HIV-1 and M-MuLV RNases H. J. Mol. Biol. 397, 161–178.
Schulz, E.C., Mehrabi, P., Müller-Werkmeister, H.M., Tellkamp, F., Jha, A., Stuart, W., Persch, E., De Gasparo, R., Diederich, F., Pai, E.F., Miller, R.J.D., 2018. The hit-and-return system enables efficient time-resolved serial synchrotron crystallography. Nat. Methods 15, 901–904.
Simanshu, D.K., Yamaguchi, Y., Park, J.H., Inouye, M., Patel, D.J., 2013. Structural basis of mRNA recognition and cleavage by toxin MazF and its regulation by antitoxin MazE in Bacillus subtilis. Mol. Cell 52, 447–458.
Singh, G., Fritz, S.M., Ranji, A., Singh, D., Boris-Lawrie, K., 2017. Isolation of cognate RNA-protein complexes from cells using oligonucleotide-directed elution. J. Vis. Exp.
Song, H., Fang, X., Jin, L., Shaw, G.X., Wang, Y.X., Ji, X., 2017. The Functional cycle of Rnt1p: five consecutive steps of double-stranded RNA processing by a eukaryotic RNase III. Structure 25, 353–363.
Song, M.S., Kumar, G., Shadrick, W.R., Zhou, W., Jeevan, T., Li, Z., Slavish, P.J., Fabrizio, T.P., Yoon, S.W., Webb, T.R., Webby, R.J., White, S.W., 2016. Identification and characterization of influenza variants resistant to a viral endonuclease inhibitor. Proc. Natl. Acad. Sci. U.S.A. 113, 3669–3674.

Sosunov, V., Sosunova, E., Mustaev, A., Bass, I., Nikiforov, V., Goldfarb, A., 2003. Unified two-metal mechanism of RNA synthesis and degradation by RNA polymerase. EMBO J. 22, 2234–2244.
Steitz, T.A., Steitz, J.A., 1993. A general two-metal-ion mechanism for catalytic RNA. Proc. Natl. Acad. Sci. U.S.A. 90, 6498–6502.
Stewart, N.K., Toth, M., Stasyuk, A., Vakulenko, S.B., Smith, C.A., 2021. Time-resolved interaction of the clostridioides difficile CDD-1 enzyme with avibactam provides new insights into the catalytic mechanism of class D β-lactamases. ACS Infect. Dis. 7, 1765–1776.
Stoddard, B.L., 2001. Trapping reaction intermediates in macromolecular crystals for structural analyses. Methods 24, 125–138.
Sun, W., Pertzev, A., Nicholson, A.W., 2005. Catalytic mechanism of Escherichia coli ribonuclease III: kinetic and inhibitor evidence for the involvement of two magnesium ions in RNA phosphodiester hydrolysis. Nucleic Acids Res. 33, 807–815.
Tekos, A., Tsagla, A., Stathopoulos, C., Drainas, D., 2000. Inhibition of eukaryotic ribonuclease P activity by aminoglycosides: kinetic studies. FEBS Lett. 485, 71–75.
Tian, L., Kim, M.S., Li, H., Wang, J., Yang, W., 2018. Structure of HIV-1 reverse transcriptase cleaving RNA in an RNA/DNA hybrid. Proc. Natl. Acad. Sci. U.S.A. 115, 507–512.
Townshend, R.J.L., Eismann, S., Watkins, A.M., Rangan, R., Karelina, M., Das, R., Dror, R.O., 2021. Geometric deep learning of RNA structure. Science 373, 1047–1051.
Unciuleac, M.C., Ghosh, S., de la Cruz, M.J., Goldgur, Y., Shuman, S., 2021. Structure and mechanism of *Mycobacterium smegmatis* polynucleotide phosphorylase. RNA 27, 959–969.
Viswanathan, M., Dower, K.W., Lovett, S.T., 1998. Identification of a potent DNase activity associated with RNase T of Escherichia coli. J. Biol. Chem. 273, 35126–35131.
Wang, Y.T., Tseng, P.H., Chen, C.L., Han, D.S., Chi, Y.C., Tseng, F.Y., Yang, W.S., 2017. Human serum RNase-L level is inversely associated with metabolic syndrome and age. Cardiovasc Diabetol 16, 46.
Ward, W.L., Plakos, K., DeRose, V.J., 2014. Nucleic acid catalysis: metals, nucleobases, and other cofactors. Chem. Rev. 114, 4318–4342.
Warnecke, J.M., Sontheimer, E.J., Piccirilli, J.A., Hartmann, R.K., 2000. Active site constraints in the hydrolysis reaction catalyzed by bacterial RNase P: analysis of precursor tRNAs with a single 3'-S-phosphorothiolate internucleotide linkage. Nucleic Acids Res. 28, 720–727.
Warnecke, J.M., Fürste, J.P., Hardt, W.D., Erdmann, V.A., Hartmann, R.K., 1996. Ribonuclease P (RNase P) RNA is converted to a Cd(2+)-ribozyme by a single Rp-phosphorothioate modification in the precursor tRNA at the RNase P cleavage site. Proc. Natl. Acad. Sci. U.S.A. 93, 8924–8928.
Wilcox, J.L., Ahluwalia, A.K., Bevilacqua, P.C., 2011. Charged nucleobases and their potential for RNA catalysis. Acc. Chem. Res. 44, 1270–1279.
Wilson, D.M., Takeshita, M., Grollman, A.P., Demple, B., 1995. Incision activity of human apurinic endonuclease (Ape) at abasic site analogs in DNA. J. Biol. Chem. 270, 16002–16007.
Wu, J., Samara, N.L., Kuraoka, I., Yang, W., 2019. Evolution of inosine-specific endonuclease v from bacterial DNase to eukaryotic RNase. Mol. Cell 76, 44–56.e43.
Xu, K., Dedic, E., Brodersen, D.E., 2016. Structural analysis of the active site architecture of the VapC toxin from Shigella flexneri. Proteins 84, 892–899.
Yang, J., Shen, C., Huang, N., 2020. Predicting or pretending: artificial intelligence for protein-ligand interactions lack of sufficiently large and unbiased datasets. Front. Pharmacol. 11, 69.
Yang, J.S., Garriga-Canut, M., Link, N., Carolis, C., Broadbent, K., Beltran-Sastre, V., Serrano, L., Maurer, S.P., 2018. rec-YnH enables simultaneous many-by-many detection of direct protein-protein and protein-RNA interactions. Nat. Commun. 9, 3747.
Yang, W., 2011. Nucleases: diversity of structure, function and mechanism. Q. Rev. Biophys. 44, 1–93.
Yi, Z., Yuan, Z., Rice, C.M., MacDonald, M.R., 2012. Flavivirus replication complex assembly revealed by DNAJC14 functional mapping. J. Virol. 86, 11815–11832.
Zegers, I., Loris, R., Dehollander, G., Fattah Haikal, A., Poortmans, F., Steyaert, J., Wyns, L., 1998. Hydrolysis of a slow cyclic thiophosphate substrate of RNase T1 analyzed by time-resolved crystallography. Nat. Struct. Biol. 5, 280–283.
Zhang, C., Konermann, S., Brideau, N.J., Lotfy, P., Wu, X., Novick, S.J., Strutzenberg, T., Griffin, P.R., Hsu, P.D., Lyumkis, D., 2018. Structural basis for the RNA-guided ribonuclease activity of CRISPR-Cas13d. Cell 175, 212–223.e217.
Zhang, C.Y., Wu, Z.Q., Yin, D.C., Zhou, B.R., Guo, Y.Z., Lu, H.M., Zhou, R.B., Shang, P., 2013. A strategy for selecting the pH of protein solutions to enhance crystallization. Acta Crystallogr. Sect. F: Struct. Biol. Cryst. Commun. 69, 821–826.
Zhao, Y., Lu, M., Zhang, H., Hu, J., Zhou, C., Xu, Q., Ul Hussain Shah, A.M., Xu, H., Wang, L., Hua, Y., 2015. Structural insights into catalysis and dimerization enhanced exonuclease activity of RNase J. Nucleic Acids Res 43, 5550-5559.
Zhao, Z.Y., McLeod, A., Harusawa, S., Araki, L., Yamaguchi, M., Kurihara, T., Lilley, D. M., 2005. Nucleobase participation in ribozyme catalysis. J. Am. Chem. Soc. 127, 5026–5027.
Zorzini, V., Mernik, A., Lah, J., Sterckx, Y.G., De Jonge, N., Garcia-Pino, A., De Greve, H., Versées, W., Loris, R., 2016. Substrate recognition and activity regulation of the Escherichia coli mRNA endonuclease MazF. J. Biol. Chem. 291, 10950–10960.
Zuo, Y., Deutscher, M.P., 1999. The DNase activity of RNase T and its application to DNA cloning. Nucleic Acids Res. 27, 4077–4082.
Zuo, Y., Deutscher, M.P., 2002. The physiological role of RNase T can be explained by its unusual substrate specificity. J. Biol. Chem. 277, 29654–29661.